Mémoire

Présenté pour obtenir le diplôme d'

HABILITATION À DIRIGER DES RECHERCHES

DE L'UNIVERSITÉ GRENOBLE ALPES
Spécialité : Physique
Arrêté ministériel : 23 novembre 1988

Présentée par

Benoît Vermersch

préparé au sein du **Laboratoire de Physique et Modélisation des Milieux Condensés** dans **l'École Doctorale de Physique de Grenoble.**

Randomized measurements for quantum technologies

HDR soutenue publiquement le **[date de la soutenance]**,
devant le jury composé de :

Avant-propos

J'ai effectué ma thèse de 2010 à 2013 sous la direction de Jean-Claude Garreau à l'université de Lille. Cette thèse avait pour but l'étude théorique des effets de la présence combinée du désordre et des interactions dans un gaz d'atomes froids.

Après ma thèse, j'ai effectué un postdoctorat de six ans (2013-2019) à l'université d'Innsbruck, au sein du groupe de Peter Zoller. Après quelques projets liés à la simulation quantique et aux réseaux quantiques, je me suis investi dans le développement de protocoles de mesure de l'intrication pour les systèmes quantiques à plusieurs corps. Recruté en septembre 2019 en tant que maître de conférences à l'université Grenoble-Alpes, je continue à travailler activement dans cette thématique. Ce manuscrit a ainsi pour but de présenter ces protocoles de mesures de l'intrication. À ce titre, je remercie tous mes collaborateurs scientifiques et tout particulièrement Andreas Elben et Peter Zoller pour leurs contributions fondamentales.

Je remercie ausi Violaine et nos enfants, Clément, Elsa, et Roméo, pour notre très belle famille.

Contents

Chapter 1

Introduction

Over the last few years, synthetic quantum systems of Rydberg atoms, trapped ions, superconducting qubits, quantum dots, etc, have reached a new era: Programmable coherent interactions can be implemented between tens of particles, and in highly tunable geometries [1]. These experimental breakthroughs raise important prospects for *quantum simulation*, where models that are fundamental for condensed matter or high-energy physics [1] can be experimentally realized, and probed with a unique level of control. Synthetic quantum systems can be also used to build *quantum computers*, with two-level atoms or anharmonic quantum circuits encoding quantum bits. These devices offer the prospect to outperform classical computers, in particular to solve "hard" classical optimization problems [2].

A central aspect for the future of quantum simulation and quantum computing is the development of experimental tools to probe a new generation of many-body quantum states, *which could not be realized so far*. Such quantum states, involving tens of particles, are described by an exponentially large Hibert space. But how to measure in an experiment the physical properties related to this enormous amount of quantum information?

The measurement problem for large-scale quantum technologies represents both a conceptual and a technological challenge. The first method that comes to mind to measure a quantum system is quantum state tomography. This consists in performing all the measurements needed to reconstruct the density matrix ρ of the system, describing all the physical properties of the quantum state. For a quantum computer with n quantum bits (qubits), the required total number of 'single-shot' measurements to measure ρ is of the order of 4^n [3]. As a consequence, tomography is typically not feasible for more than $8-10$ qubits [4].

Several strategies have been proposed to reduce the number of measurements to perform state tomography. If the state is close to a pure state, i.e., the underlying density matrix has low rank, one can use compressed sensing methods to reduce the number of measurements [3]. If the state has a low level of entanglement, we can write the density matrix in good approximation as the contraction of a Matrix-Product-State (MPS). MPS tomography is 'efficient' in the sense that the number of measurements is polynomial in system size [5, 6]. Finally, if we assume that the state can be described by an ansatz with few parameters, we can rely on neural networks to reconstruct the density matrix based on few measurements compared to standard tomography [7]. While we have seen in recent years a very significant effort to extend techniques based on machine learning-based methods, it is not clear at the moment which level of assumption (mixed state, positive coefficients, low entanglement) is required to make these algorithms relevant in different physical scenarios [8].

Approach	Type of measured quantities	Applicability
Standard Tomography	Density Matrix ρ	Small systems
Compressed sensing, MPS and Neural Network Tomography	State or Density matrix	Designed for specific states
Randomized benchmarking	Error rate	
Entanglement Witnesses	Correlations, Bell inequalities,...	Designed for specific states
Direct Fidelity estimation Cross-Entropy benchmarking	Fidelity w.r.t theory state	The state can be represented classically
Multiple copies	Entanglement entropies	Requires two identical systems
Randomized measurements	Entanglement entropies, fidelities, scrambling, topological invariants,...	Moderate partition sizes

Figure 1.1: Non-exhaustive list of methods for probing quantum technologies. Our approach is randomized measurements, with the goal to measure, without multiple copies, universal physical quantities associated with entanglement.

1.1 Benchmarking quantum computers

Quantum computers now operate in the regime of the 'quantum advantage' with more than 50 qubits [9]. This means that quantum computers have not offered yet a practical advantage over classical computers. However, they can implement a quantum circuit that cannot be classically simulated for a reasonable amount of time, and hardware resources. Such claim of quantum advantage could not have been made without the possibility to *benchmark* quantum computers. This consists in assessing the level of errors in the realization of the quantum circuit. As quantum state tomography is not an option for such large systems, one can measure such errors using different approaches. In randomized benchmarking (RB) [10], the strategy consists in using random circuits that implement a gate sequence that is then time-inverted. Emerson and colleagues have shown that average gate errors can be extracted from the overlap between the final and the initial state (overlap one meaning that no errors occured), and that this estimation can be realized in large quantum devices. This provides a direct test of the *average* expected performance of a quantum computer that complements approaches based on listing quantum hardware specificities (e.g., 'the quantum volume' used by the companies IBM [11] and Honeywell [12]). However, RB is not relevant for assessing the faithful realization of a *single* quantum circuit (or Hamiltonian, as encountered in quantum simulation).

Another direct test of quantum computers consists in measuring the fidelity in the preparation of a given quantum state [13, 9, 14]. Obviously, this approach cannot be applied in the regime of quantum advantage, as the ideal state must be calculated and represented classically in order to allow for comparison with the quantum device.

1.2 Measuring physics properties associated with entanglement

Instead of trying to reconstruct the quantum state or to benchmark errors, one can also probe many-body quantum systems by measuring physical properties, independently of a certain type of quantum computing architecture and of classical simulations. In particular, I have been interested

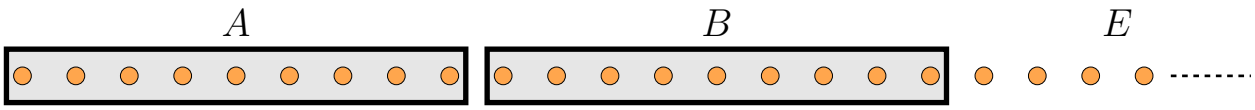

Figure 1.2: A quantum system, here represented as a lattice system, with a bipartition A and B, and environnement E.

over the last years in the challenge of probing entanglement, which describes to which extent a many-body quantum state cannot be written as a classical 'product' state (say of two spatially separated subsystems). First, the idea of measuring entanglement is very relevant to benchmark quantum computers, as it demontrates the most elementary of the quantum properties, independently of the model, assumptions on the state, classical simulations, etc. We also know that the states with a low level of entanglement are the ones that can be simulated by a classical computer [15]. This means that only quantum computers featuring a large amount of entanglement can indeed offer new possibilities w.r.t. classical devices. Finally, on the physics side, entanglement can also unravel universal properties of the dynamics of quantum computers, deep in the regime of quantum advantage [16].

In the framework of quantum simulation of condensed matter and high-energy physics theories, the universal properties of entanglement describing quantum matter in-/(out-of-) equilibrium have raised significant interest. In particular, the physical quantities associated with entanglement have been shown to have the ability to describe as 'non-local order parameters' key features of many quantum phases and quantum phase transitions [15, 17]. We describe some illustrative examples below.

1.2.1 Bipartite entanglement

Let us now introduce the concept of bipartite entanglement. For this, one considers a quantum system, which is divided into two parts A and B, e.g a set of spins 1/2 (qubits), c.f Fig. 1.2. We also denote E the environnement, so that we can consider, without any loss of generality, that the combined state of A, B and E is described by a wavefunction $|\psi\rangle$ of a pure quantum state. For example, in the case of decoherence affecting the system, phonons, photons,..., are included in the environment part E of the wavefunction.

All the physical properties of A and B are described by the reduced density matrix

$$\rho_{AB} = \mathrm{tr}_E(|\psi\rangle\langle\psi|), \tag{1.1}$$

which is obtained by tracing all the degree of freedoms of the environment E. Similarly, we define the reduced density matrices $\rho_A = \mathrm{tr}_{BE}(|\psi\rangle\langle\psi|)$, and $\rho_B = \mathrm{tr}_{AE}(|\psi\rangle\langle\psi|)$ of A and B, respectively.

Pure states

The concept of bipartite entanglement between A and B can be easily understood by first assuming that the reduced state ρ_{AB} is pure: $\rho_{AB} = |\psi_{AB}\rangle\langle\psi_{AB}|$ (or, equivalently, that we can 'factorize' the state of the environment, i.e., $|\psi\rangle = |\psi_{AB}\rangle \otimes |\psi_E\rangle$).

A pure state is said to be separable if $|\psi_{AB}\rangle$ can be written as a product state [18].

$$|\psi_{AB}\rangle = |\psi_A\rangle \otimes |\psi_B\rangle\,. \tag{1.2}$$

Conversely, a state which is not separable is said to be *entangled*.

Note that any pure quantum state can always be decomposed via a Schmidt decomposition as a mixture of product states [18]

$$|\psi_{AB}\rangle = \sum_i \sqrt{\lambda^{(i)}} e^{i\varphi^{(i)}} |\psi_A^{(i)}\rangle \otimes |\psi_B^{(i)}\rangle \,, \tag{1.3}$$

with ($\lambda^{(i)}$ the Schmidt spectrum. Here, $\sum_i \lambda_i = 1$ and the states $|\psi_{A,B}^{(i)}\rangle$ are normalized and orthogonal to each other. According to the decomposition, a separable state is made of a single Schmidt value $\lambda_1 = 1$, while entangled states possess at least two non-zero Schmidt values. The Schmidt decomposition plays a key role for determining the ability for classical computers to simulate quantum system: Tensor-network algorithms can only handle a given number of Schmidt values, i.e., this means they can only simulate the dynamics of 'low' entangled states [19].

Mixed states

A mixed state is said to be separable if it can be written as a sum of product states [18]

$$\rho_{AB} = \sum_k p_k \left(\rho_A^{(k)} \otimes \rho_B^{(k)} \right), \tag{1.4}$$

with positive coefficients $0 \leq p_k \leq 1$. Conversely, a mixed state that cannot be written as in Eq. (1.4) is declared to be entangled.

Consider an arbitrary quantum state ρ_{AB}. The question of whether a decomposition of the form of Eq. (1.4) exists, i.e, whether the state is entangled or not is one of the most important problems in quantum information theory [18]. Let us present now different strategies that were introduced to address the challenge of detecting and quantifying entanglement.

1.2.2 Entanglement witnesses

Certain expectation values of observables, known as *entanglement witnesses*, can be used to demonstrate that a state is entangled [18]. When the state under study can be written analytically, it is in particular possible to derive an entanglement witness, such as a Bell inequality, which can be then measured in an experiment to certify the presence of entanglement [20], while relaxing certain assumptions on the measurement devices [21, 22]. It is also possible to collect data in the experiment that can be used to derive numerically a potential entanglement witness [23].

In order to simplify the experimental task of detecting entanglement, and having in mind the scenario of quantum simulation and quantum computation with many different types of a priori unknown entangled quantum states being created, it seems thus important to complement the approach of entanglement witnessess, and consider entanglement tests that can detect entanglement without prior knowledge on the state.

1.2.3 Detecting entanglement via entanglement entropies

In contrast to entanglement witnesses, entanglement entropies can be used in a complete state-agnostic manner. More importantly, entanglement entropies also *quantify* the amount of entanglement present in a system.

First, the concept of bipartite entanglement can be easily formulated in terms of entanglement entropies [15], such as the von-Neumann entropy

$$S(\rho) = -\mathrm{tr}(\rho \log(\rho)), \tag{1.5}$$

and, more generally, the Rényi entropies

$$S_\alpha(\rho) = \frac{1}{1-\alpha} \log \mathrm{tr}(\rho^\alpha), \tag{1.6}$$

which includes the von-Neuman entropy $S_1 \equiv \lim_{\alpha\to 1} S_\alpha = S$. Here, we use $\log = \log_2$.

Pure states

For pure states, it is convenient to consider the Schmidt decomposition Eq. (1.3), and write the reduced density matrix of a subsystem $X = A, B$ (by tracing over the complement)

$$\rho_X = \sum_i \lambda^{(i)} \left|\psi_X^{(i)}\right\rangle \left\langle\psi_X^{(i)}\right|. \tag{1.7}$$

Hence, a separable state, characterized by a single Schmidt value $\lambda^{(i)} = 1$, leads to pure reduced states $\mathrm{tr}(\rho_X^2) = 1$. Conversely, entangled states give rise to mixed reduced states $\mathrm{tr}(\rho_X^2) < 1$. Moreover, as the entropies of the reduced states are

$$S_\alpha(\rho_X) = \frac{1}{1-\alpha} \log \sum_i \left(\lambda^{(i)}\right)^\alpha. \tag{1.8}$$

Therefore a pure state is entangled if and only if the entanglement entropies of the reduced states are larger than zero.

The von-Neuman entropy satisfies the required mathematical properties, associated with an *entanglement measure* [24]. In particular, the von-Neuman entropy is a strict entanglement monotone, which means that it cannot grow under local operation and classical communication (LOCC) operations. Other Rényi entropies for $\alpha > 1$ provide bounds to the von-Neumann entropy, and they also satisfy some of the properties of an entanglement measure (like monotonicity under LOCC [24]).

Mixed states

For mixed states, entanglement entropies are not entanglement measures, but they can still be used for detecting entanglement [25, 26, 18]. We restrict here to the case of the second Rényi entropy. If a state is separable then we can prove that it implies that

$$S_2(\rho_{AB}) \geq S_2(\rho_A), \tag{1.9}$$

with the same inequality holding for $S_2(\rho_B)$. The proof consists in using Eq. (1.4), and write

$$\mathrm{tr}(\rho_{AB}^2) \quad = \quad \sum_{k,k'} p_k p_{k'} \mathrm{tr}(\rho_A^{(k)} \rho_A^{(k')}) \mathrm{tr}(\rho_B^{(k)} \rho_B^{(k')}). \tag{1.10}$$

Let us now write the eigenstates decomposition of the reduced density matrix

$$\rho_B^{(k)} = \sum_i \lambda_B^{(i,k)} \left|\psi_B^{(i,k)}\right\rangle \left\langle\psi_B^{(i,k)}\right|, \tag{1.11}$$

with $\sum_i \lambda_B^{(i,k)} = 1$. This allows us to bound the overlap terms as

$$\mathrm{tr}(\rho_B^{(k)} \rho_B^{(k')}) = \sum_{i,i'} \lambda_B^{(i,k)} \lambda_B^{(i',k')} |\left\langle\psi_B^{(i,k)}\right| \left.\psi_B^{(i',k')}\right\rangle|^2 \leq \sum_{i,i'} \lambda_B^{(i,k)} \lambda_B^{(i',k')} = 1. \tag{1.12}$$

Similarly, writing the eigenstate decompositions for the matrices $\rho_A^{(k)}$, we find that $\mathrm{tr}(\rho_A^{(k)}\rho_A^{(k')}) \geq 0$, and therefore

$$\mathrm{tr}(\rho_{AB}^2) \leq \sum_{k,k'} p_k p_{k'} \mathrm{tr}(\rho_A^{(k')}\rho_A^{(k')}) = \mathrm{tr}(\rho_A^2), \tag{1.13}$$

which finally implies Eq. (1.9). Conversely, if $S_2(\rho_A) > S_2(\rho_{AB})$, then the state is entangled. Note that this is not a necessary condition for bipartite entanglement: i.e., not all entangled states satisfy $S_2(\rho_A) > S_2(\rho_{AB})$.

1.2.4 Entanglement entropies in many-body physics

In the condensed matter context, entanglement entropies are able to extract universal entanglement properties of many-body quantum states. Let us present a few illustrative examples. Here, we will consider that the state $\rho_{AB} = |\psi_{AB}\rangle\langle\psi_{AB}|$ of the system AB is pure.

The scaling of entanglement of many-body ground states: Area law

Consider a D-dimensional many-body system S, e.g., spin 1/2 particles on a lattice geometry, and in the groundstate $|\psi\rangle$ of a many-body Hamiltonian H (here $S = AB$). We now consider two assumptions: the interactions between particles has a finite spatial range, and the system is not at a quantum phase transition point. In this case, the entanglement entropy of the reduced density matrix ρ_A of a hypercube $A \subset S$ of size ℓ^D (see schematic Fig. 1.3 for $D = 2$) scales with the area ℓ^{D-1} of A [15]

$$S_\alpha(\rho_A) \propto \ell^{D-1}. \tag{1.14}$$

The area law has only been formally proven for certain exactly solvable models [15], such as with non-interacting particles, or in integrable topological models: e.g., the Affleck, Lieb, Kennedy and Tasaki model (AKLT) and the toric code. However, the area law can indeed be understood phenomenologically, as a consequence of equilibrium, which implies *the existence of a finite correlation length* ℓ_c.

Consider for concreteness a two-dimensional lattice model, c.f., Fig. 1.3a). Having the existence of a finite correlation length means that a site i that belongs to A can only be entangled with sites j that are separated by a distance $|\mathbf{r}_i - \mathbf{r}_j|$ smaller than ℓ_c. Summing all contributions, the subsystem A can only share entanglement with a number of B sites that live in a volume $V = \ell_c \ell^{D-1}$, c.f., Fig. 1.3a). When we trace out these B sites, we form a reduced density ρ_A with entropy $S_\alpha(\rho_A) \sim V = \ell_c \ell^{D-1}$, which is the area law.

The area law is a universal signature of equilibrium for many-body states, which can be verified numerically, see an example obtained in Fig. 1.3b). The area law has also direct applications for the numerical simulation of many-body systems. With tensor-networks in particular, the relatively low entanglement level of area-law states makes the simulations of large-scale many-body quantum systems feasible [19].

As we show now, sub-leading corrections to the area law can also have a universal behavior, which are independent of the microscopic details of the system, and which can be thus extracted numerically, or measured, in order to establish phase diagrams.

Universal corrections to the area law: central charge

The first type of universal contributions to the area law is related to a quantum phase transition in one spatial dimension. As the correlation length diverges as one approaches the transition point, the

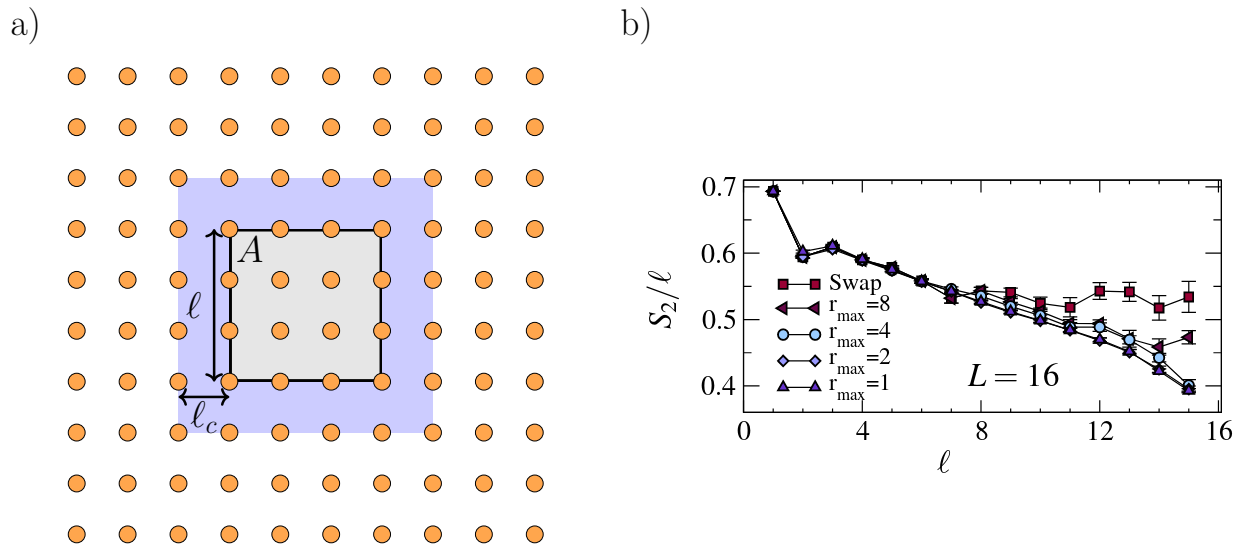

Figure 1.3: a) Schematic of the different lenghts involved in the scaling of entanglement in the ground state of a many-body system. The entanglement entropy of ρ_A scales with the area of A. b) Numerical demonstration of the area law scaling in the two-dimensional Heisenberg model via quantum Monte-Carlo methods [27].

system can be described by a scale-invariant quantum field theory associated with the universality class of the phase transition [28]. In particular, the divergence of the correlation length results in an entanglement entropy which scales as

$$S_\alpha(\rho_A) = f_\alpha(c)\log(\ell), \tag{1.15}$$

with f_α is a known function of α, and c is the central charge associated with the universality class. The central charge is now routinely extracted in numerical simulations to identify the universality class of a quantum phase transition, see e.g., Ref. [29] and Fig. 1.4a).

Universal corrections to the area law: topological entanglement entropy

Topological phases of matter are quantum phases that lie beyond the Landau symmetry-breaking paradigm, i.e., they cannot be identified from a local order parameter (magnetization, spin correlations, etc). The entanglement entropy has emerged as one of the most relevant candidates to serve as *non-local* order parameter [30, 31, 32, 33]. In systems with intrinsic topological order, there indeed exists a peculiar *negative* universal contribution to the area law

$$S_\alpha(\rho_A) = -\gamma + \beta\ell. \tag{1.16}$$

The term γ is called the topological entanglement entropy [30, 31, 32], and results from 'long-range entanglement', which is a certain type of entanglement that can be only generated from a physical operation acting on the whole system, and which is conjectured to be the distinctive feature of topological order [34]. The topological entanglement entropy is one numerical diagnosis of reference for topological order in numerical simulations, see example in Fig. 1.4, and could also be used in the future to probe topological order in quantum simulation experiments.

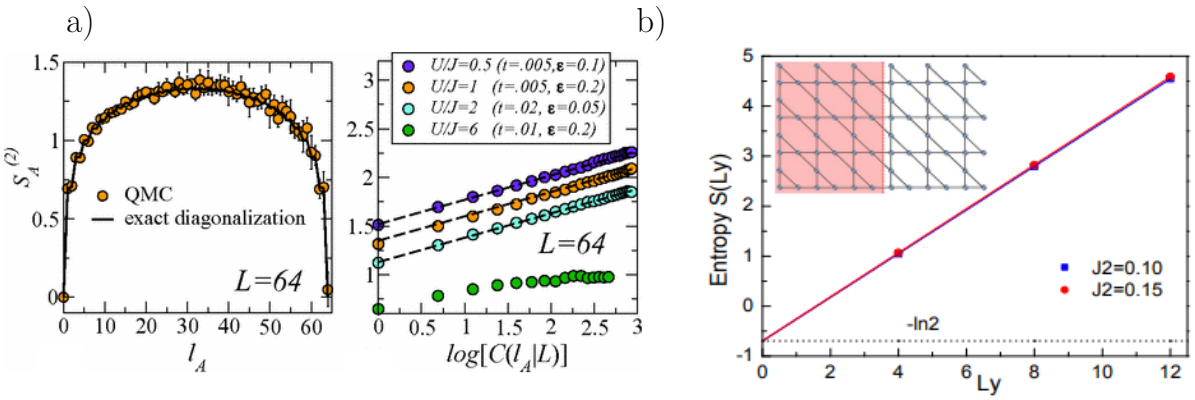

Figure 1.4: a) Numerical observation of the logarithmic scaling of entanglement at a quantum phase transition [29]. b) Numerical extraction via tensor-network algorithms of the topological entanglement entropy γ in a non-integrable toric-code model [35].

Entanglement entropies out-of-equilibrium

The ability for entanglement entropies to reveal the distinctive features of a many-body system is not restricted to the scenario of equilibrium. The dynamical process of thermalization, i.e., the question of how a state *enters* the regime of equilibrium, can also be revealed by entanglement entropies.

Consider for example an initial non-entangled state $|\psi_0\rangle$, which is then time-evolved in one spatial dimension with a unitary operation, $|\psi(t)\rangle = U(t)\,|\psi_0\rangle$. The main questions related to thermalization are: how does a reduced system A equilibrate to a thermal state based on his interaction with the rest of the system B? And how is this manifested in terms of the time evolution of thermodynamical quantitites, such as entanglement entropies $S_\alpha(\rho_A)$?

Some of the universal features of quantum thermalization have been understood based on quantum field theory [36]. In the course of time-evolution, unitary dynamics can be described in terms of elementary excitations (for instance, these are called magnons for spin-systems). These *quasi-particles* propagate ballistically, entangling regions that are more and spatially separated. As a consequence, the correlation length $\ell_c(t) \propto t$ of the system grows linearly with time, and the entanglement entropy $S_\alpha(\rho_A) \sim \ell_c(t)$ follows the same behavior. At late times, the entanglement entropy reaches a 'volume-law' plateau $S \sim \ell$ associated with thermal equilibrium, see Fig. 1.5a) for an illustration.

Over the last decades, we have understood that the picture of thermalization described above does not apply to all systems. In the presence of spatial inhomogeneities for example, quasi-particles do not propagate ballistically due to destructive quantum interference effects. This leads to a drastic slow-down of the thermalization dynamics known as 'many-body localization' [37]. Remarkably, entanglement entropies have been shown to display in this case a universal logarithmic growth [38], c.f., Fig. 1.5b).

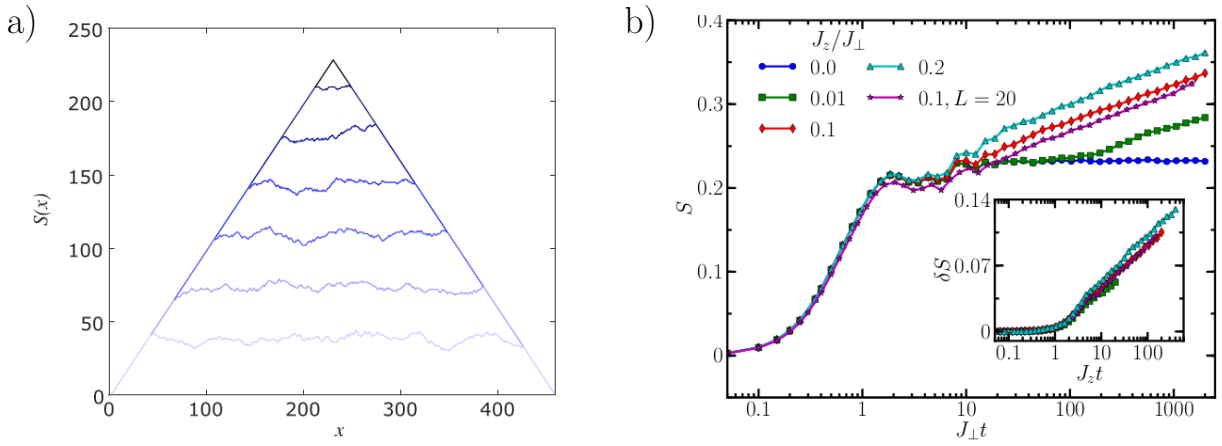

Figure 1.5: a) Linear entanglement growth in a unidimensional quantum system [16]. At a given time (color), the von-Neumann entropy features a characteristic area-law plateau associated with the existence of a finite correlation length $\ell_c(t)$. As time increases, the height of this plateau linearly increases, as $\ell_c(t) \sim vt$. b) Logarithmic growth of entanglement entropy in a many-body localized system [38].

1.3 How to measure entanglement entropies?

1.3.1 Measurement protocol with multiple copies

We have seen that entanglement entropies can detect and quantify entanglement of many-body systems. How can we measure these quantities in an experiement? A first breakthrough in this context was to realize that entanglement entropies can be measured by creating in an experiment two identical copies $\rho_A \otimes \rho_A$ of a quantum system [39, 40]. By making an interference between these copies, one can access the second Rényi entanglement entropies $S_2(\rho_A)$.

This protocol has been demonstrated experimentally in two remarkable experiments [41, 42], see also Fig. 1.6. In these experiments, a degenerate atomic Bose gas was loaded into two adjacent unidimensional optical lattices, forming two identical copies $\rho_A \otimes \rho_A$ of a unidimensional Bose Hubbard system. The interference between these two copies was realized via atomic tunneling.

This protocol demonstrated remarkable capabilities of atomic quantum technologies for measuring entanglement, but raised fundamental questions in terms of general applicability. First, the two copies must be exactly prepared identically and subject to the exact same Hamiltonians, an operation which becomes extremely challenging when dealing with large many-body systems. More importantly, very few platforms have indeed the possibility to implement and interfere two copies of their setups. In particular, the effort and investment that are already needed to implement a single quantum simulator or computer are so significant that it became highly desirable to develop new measurement protocols that do not require having such two copies.

1.3.2 Statistics instead of copies: Randomized measurements

Surprisingly and recently, we understood that we can also measure entanglement entropies with 'single copies'. To introduce this approach, it is intructive to first recall how a 'standard' measurement is performed, see Fig. 1.7. For measuring an observable O, one takes projective measurements in the eigenbasis $\{s\}$ of O, in order to provide an estimation of an expectation value $\langle O \rangle = \mathrm{Tr}(\hat{O}\rho_A) = \sum_s O(s) \langle s| \rho_A |s\rangle$, which is a linear function of the density matrix. For instance,

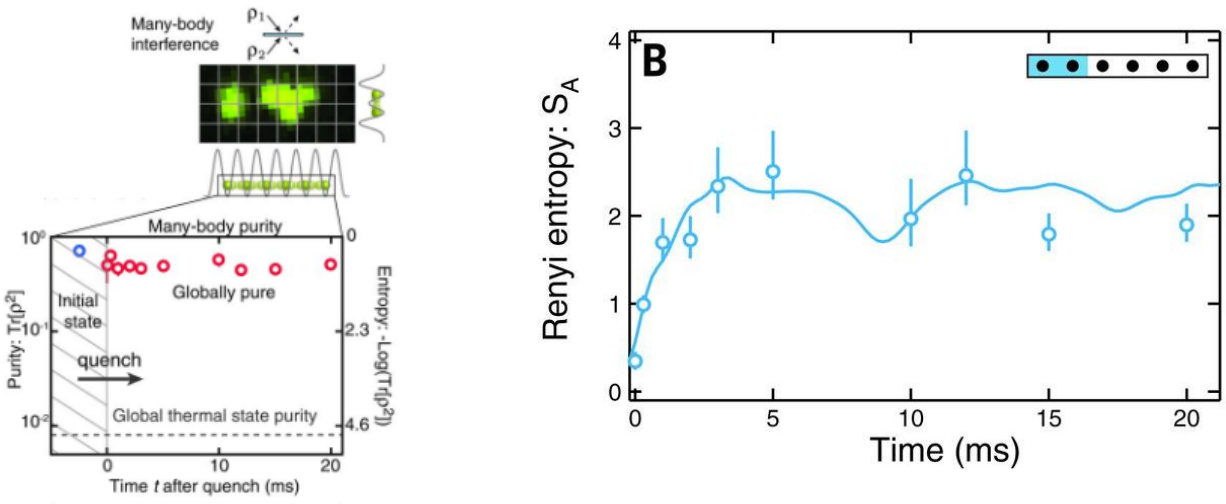

Figure 1.6: Measurement of the second Rényi entropy in an ultracold atom system implementing the Bose-Hubbard model [42].

for the demonstration of quantum advantage by Google AI, a set of bit-strings $\{s_i\}$ were collected to construct estimations of spin probabilities [9].

In order to access *non-linear* properties of the density matrix ρ_A, such as Rényi entropies, this procedure is obviously not sufficient, and we need another ingredient. We have seen above that the first approach to measure non-linear properties of ρ_A consists in duplicating physically the system [39, 40, 41]. The second approach, **randomized measurements**, consists in replacing these physical copies *by successive realizations in an experiment of a single quantum system, and applying different random operations u before the measurement.*

The idea of randomized measurements has been first introduced by van Enk and Beenakker in the quantum information context [44]. Randomized measurements give access to measurement probabilities $P_{u,\rho_A}(s) = \langle s|\, u\rho_A u^\dagger \,|s\rangle$ that are random numbers depending on the random unitary matrix u, and of the state ρ_A. The key result from van Enk and Benakeer is that the statistics of the random measurements $P_{u,\rho_A}(s)$, obtained by sampling a certain number of random unitaries u over the circular unitary ensemble (CUE), gives access to entanglement Rényi entropies. In particular, for the second Rényi entropy $S_2(\rho_A) = -\log[\mathrm{Tr}(\rho_A^2)]$, the mapping between entanglement entropy and statistical correlations takes the form of a remarkable simple expression

$$S_2(\rho_A) = -\log[(d+1)\sum_s \overline{P_{u,\rho_A}(s)^2} - 1],$$

with d the Hilbert space dimension, and $\overline{\ }$ the ensemble average of the unitaries over the CUE [44].

1.4 Outline of the manuscript

This manuscript presents our contributions to the field of randomized measurements.

In chapter 2, we present our first constributions, the main result being the first protocol to measure entanglement entropies of qubit systems that only relies in local random unitaries [45], and the corresponding first experimental demonstration of randomized measurements using a trapped ion quantum simulator [43]. I also discuss the results presented in our works [46, 47].

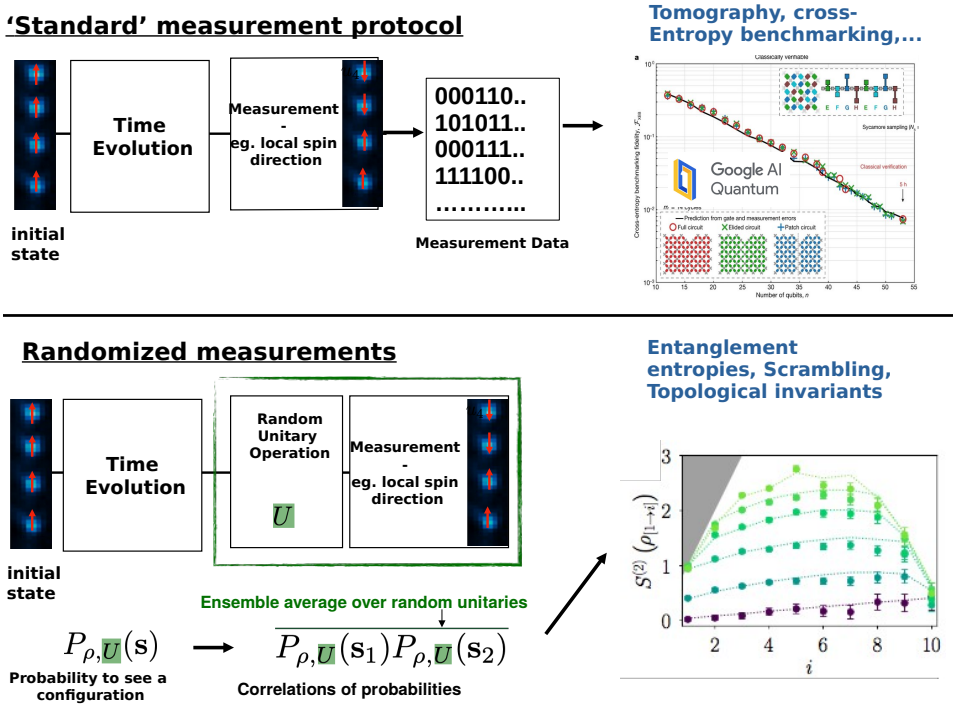

Figure 1.7: Comparison between standard and randomized measurements protocols. In a standard protocol, a certain observable is accessed by projective measurement. Right panel: illustration with the quantum advantage experiment by Google AI Quantum [9] based on measuring bit-string probabilities, and performing cross-entropy benchmarking with classical simulations. In a randomized measurement prococol, a random unitary operation is applied prior to the measurement. This gives access to a statistical distribution of measurements, which can be then used to access quantities that are not quantum observables, such as entanglement entropies. Right panel: experimental demonstration of RM in a 10 qubit trapped ion quantum simulator [43].

In chapter 3, I will show, using the graphical approach introduced in chapter 2, how to generalize our protocols to measure new quantities beyond entanglement entropies. This will cover the protocol to characterize the 'scrambling' of quantum information [48], and the corresponding experimental observation in a many-body system with local interactions [49]. I will then show that randomized measurements provide protocols for measuring many-body topological invariants of symmetry protected topological phases [50], and two-dimensional topological fractional Chern insulators [51]. Finally, I will show that randomized measurements can also verify quantum computation tasks by measuring state-fidelities between two quantum states prepared in two different experiments [14].

In chapter 4, I will show that randomized measurements protocols can be reinterpreted in the framework of 'shadow tomography' [52, 53]. This formalism allowed us to derive and demontrate protocols to detect and quantify entanglement via the positive-partial-transpose (PPT) condition [14].

1.5 Publications discussed in this manuscript

Brydges, T., Elben, A., Jurcevic, P., Vermersch, B., Maier, C., Lanyon, B. P., Zoller, P., Blatt, R. & Roos, C. F. (2019), 'Probing Rényi entanglement entropy via randomized measurements', *Science* **364**(6437), 260–263.
URL: *http://dx.doi.org/10.1126/science.aau4963*

Cian, Z.-P., Dehghani, H., Elben, A., Vermersch, B., Zhu, G., Barkeshli, M., Zoller, P. & Hafezi, M. (2021), 'Many-Body Chern Number from Statistical Correlations of Randomized Measurements', *Physical Review Letters* **126**(5), 050501.
URL: *https://link.aps.org/doi/10.1103/PhysRevLett.126.050501*

Elben, A., Kueng, R., Huang, H.-Y. R., van Bijnen, R., Kokail, C., Dalmonte, M., Calabrese, P., Kraus, B., Preskill, J., Zoller, P. & Vermersch, B. (2020), 'Mixed-State Entanglement from Local Randomized Measurements', *Physical Review Letters* **125**(20), 200501.
URL: *http://dx.doi.org/10.1103/PhysRevLett.125.200501*

Elben, A., Vermersch, B., Dalmonte, M., Cirac, J. I. & Zoller, P. (2018), 'Rényi Entropies from Random Quenches in Atomic Hubbard and Spin Models', *Physical Review Letters* **120**(5), 050406.
URL: *https://link.aps.org/doi/10.1103/PhysRevLett.120.050406*

Elben, A., Vermersch, B., Roos, C. F. & Zoller, P. (2019), 'Statistical correlations between locally randomized measurements: A toolbox for probing entanglement in many-body quantum states', *Physical Review A* **99**(5), 052323.
URL: *https://link.aps.org/doi/10.1103/PhysRevA.99.052323*

Elben, A., Vermersch, B., van Bijnen, R., Kokail, C., Brydges, T., Maier, C., Joshi, M. K., Blatt, R., Roos, C. F. & Zoller, P. (2020), 'Cross-Platform Verification of Intermediate Scale Quantum Devices', *Physical Review Letters* **124**(1), 010504.
URL: *https://link.aps.org/doi/10.1103/PhysRevLett.124.010504*

Joshi, M. K., Elben, A., Vermersch, B., Brydges, T., Maier, C., Zoller, P., Blatt, R. & Roos, C. F. (2020), 'Quantum Information Scrambling in a Trapped-Ion Quantum Simulator with Tunable Range Interactions', *Physical Review Letters* **124**(24), 240505.
URL: *https://link.aps.org/doi/10.1103/PhysRevLett.124.240505*

Vermersch, B., Elben, A., Dalmonte, M., Cirac, J. I. & Zoller, P. (2018), 'Unitary n -designs via random quenches in atomic Hubbard and spin models: Application to the measurement of Rényi entropies', *Physical Review A* **97**(2), 023604.
URL: *https://link.aps.org/doi/10.1103/PhysRevA.97.023604*

Vermersch, B., Elben, A., Sieberer, L. M., Yao, N. Y. & Zoller, P. (2019), 'Probing Scrambling Using Statistical Correlations between Randomized Measurements', *Physical Review X* **9**(2), 021061.
URL: *http://dx.doi.org/10.1103/PhysRevX.9.021061*

1.6 Publications not discussed in this manuscript

Celi, A., Vermersch, B., Viyuela, O., Pichler, H., Lukin, M. D. & Zoller, P. (2020), 'Emerging Two-Dimensional Gauge Theories in Rydberg Configurable Arrays', *Physical Review X* **10**(2), 021057.
URL: *https://link.aps.org/doi/10.1103/PhysRevX.10.021057*

Cherroret, N., Vermersch, B., Garreau, J. C. & Delande, D. (2014), 'How Nonlinear Interactions Challenge the Three-Dimensional Anderson Transition', *Physical Review Letters* **112**(17), 170603.
URL: *https://link.aps.org/doi/10.1103/PhysRevLett.112.170603*

Dalmonte, M., Vermersch, B. & Zoller, P. (2018), 'Quantum simulation and spectroscopy of entanglement Hamiltonians', *Nature Physics* **14**(8), 827–831.
URL: *http://www.nature.com/articles/s41567-018-0151-7*

Dlaska, C., Vermersch, B. & Zoller, P. (2017), 'Robust quantum state transfer via topologically protected edge channels in dipolar arrays', *Quantum Science and Technology* **2**(1), 015001.
URL: *https://iopscience.iop.org/article/10.1088/2058-9565/2/1/015001*

Grankin, A., Guimond, P. O., Vasilyev, D. V., Vermersch, B. & Zoller, P. (2018), 'Free-space photonic quantum link and chiral quantum optics'.
URL: *https://link.aps.org/doi/10.1103/PhysRevA.98.043825*

Guimond, P. O., Grankin, A., Vasilyev, D. V., Vermersch, B. & Zoller, P. (2019), 'Subradiant Bell States in Distant Atomic Arrays', *Physical Review Letters* **122**(9), 093601.
URL: *https://link.aps.org/doi/10.1103/PhysRevLett.122.093601*

Guimond, P.-O., Vermersch, B., Juan, M. L., Sharafiev, A., Kirchmair, G. & Zoller, P. (2020), 'A unidirectional on-chip photonic interface for superconducting circuits', *npj Quantum Information* **6**(1), 32.
URL: *http://www.nature.com/articles/s41534-020-0261-9*

Mazloom, A., Vermersch, B., Baranov, M. A. & Dalmonte, M. (2017), 'Adiabatic state preparation of stripe phases with strongly magnetic atoms', *Physical Review A* **96**(3), 033602.
URL: *https://link.aps.org/doi/10.1103/PhysRevA.96.033602*

Ramos, T., Vermersch, B., Hauke, P., Pichler, H. & Zoller, P. (2016), 'Non-Markovian dynamics in chiral quantum networks with spins and photons', *Physical Review A* **93**(6), 062104.
URL: *https://link.aps.org/doi/10.1103/PhysRevA.93.062104*

Schuetz, M. J. A., Vermersch, B., Kirchmair, G., Vandersypen, L. M. K., Cirac, J. I., Lukin, M. D. & Zoller, P. (2019), 'Quantum simulation and optimization in hot quantum networks', *Physical Review B* **99**(24), 241302.
URL: *https://link.aps.org/doi/10.1103/PhysRevB.99.241302*

Vermersch, B. (2016), 'Anisotropy and state mixing in the interactions between Rydberg states', *The European Physical Journal Special Topics* **225**(15-16), 2977–2991.
URL: *http://link.springer.com/10.1140/epjst/e2015-50337-x*

Vermersch, B., Delande, D. & Garreau, J. C. (2020), 'Bogoliubov excitations in the quasiperiodic kicked rotor: Stability of a kicked condensate and the quasi–insulator-to-metal transition', *Physical Review A* **101**(5), 053625.
URL: *https://link.aps.org/doi/10.1103/PhysRevA.101.053625*

Vermersch, B. & Garreau, J. C. (2012), 'Interacting ultracold bosons in disordered lattices: Sensitivity of the dynamics to the initial state', *Physical Review E* **85**(4), 046213.
URL: *http://link.aps.org/doi/10.1103/PhysRevE.85.046213*

Vermersch, B. & Garreau, J. C. (2013*a*), 'Decoherence effects in the dynamics of interacting ultracold bosons in disordered lattices', *The European Physical Journal Special Topics* **217**(1), 109–119.
URL: *http://link.springer.com/10.1140/epjst/e2013-01760-0*

Vermersch, B. & Garreau, J. C. (2013*b*), 'Spectral description of the dynamics of ultracold interacting bosons in disordered lattices', *New Journal of Physics* **15**(4), 045030.
URL: *http://stacks.iop.org/1367-2630/15/i=4/a=045030*

Vermersch, B. & Garreau, J. C. (2015), 'Emergence of nonlinear behavior in the dynamics of ultracold bosons', *Physical Review A* **91**(4), 043603.
URL: *https://link.aps.org/doi/10.1103/PhysRevA.91.043603*

Vermersch, B., Glaetzle, a. W. & Zoller, P. (2015), 'Magic distances in the blockade mechanism of Rydberg p and d states', *Physical Review A* **91**(2), 023411.
URL: *http://link.aps.org/doi/10.1103/PhysRevA.91.023411*

Vermersch, B., Guimond, P.-O., Pichler, H. & Zoller, P. (2017), 'Quantum State Transfer via Noisy Photonic and Phononic Waveguides', *Physical Review Letters* **118**(13), 133601.
URL: *https://link.aps.org/doi/10.1103/PhysRevLett.118.133601*

Vermersch, B., Ramos, T., Hauke, P. & Zoller, P. (2016), 'Implementation of chiral quantum optics with Rydberg and trapped-ion setups', *Physical Review A* **93**(6), 063830.
URL: *https://link.aps.org/doi/10.1103/PhysRevA.93.063830*

Vogell, B., Vermersch, B., Northup, T. E., Lanyon, B. P. & Muschik, C. A. (2017), 'Deterministic quantum state transfer between remote qubits in cavities', *Quantum Science and Technology* **2**(4), 045003.
URL: *https://iopscience.iop.org/article/10.1088/2058-9565/aa868b*

Chapter 2

Randomized measurements via the graphical approach

In this chapter, we present a general theory framework to describe randomized measurement protocols. The main result derived from this framework is a randomized measurement protocol for qubit systems using local random unitaries [45], which was experimentally demonstrated in Ref. [43].

2.1 Tensor description of a quantum state

We would like here to describe a quantum state of N 'entities' by a wavefunction

$$|\psi\rangle = \sum_{s_1,\ldots,s_N} \psi_{s_1,\ldots,s_N} |s_1\rangle \otimes \cdots \otimes |s_N\rangle \,, \tag{2.1}$$

with indices $s_i = 1, \ldots, d$, d being the internal dimension of the entities. The object $\psi_{s_1,\ldots,s_N}$ is a N-leg tensor that can be represented and manipulated graphically, see below. The tensor is represented as a box with N horizontal lines representing the N indices. Such a graphical description is commonly used in particular in the tensor-network framework [19]. In our description, an entity represented by an index i does not necessarily represent a single physical constituent. For example, we can consider local decompositions of a system of L qubits, with $N = L$, and $d = 2$, each index $s_i = 0, 1$ representing the state of one qubit. But, we can also describe the same system 'globally', i.e., as a single entity $N = 1$ with internal dimension $d = 2^L$, and 'digital' indices $s = s_1 = 1, \ldots, 2^L$. One can also include in this description an environment acting as decoherence, etc.

The distinction between local ($N > 1$) and global ($N = 1$) descriptions of a quantum state will be essential for our discussion. While the van Enk and Beenakker approach [44] considers the global description $N = 1$ to introduce randomized measurements, we have developed a local framework, which allowed us to provide new measurement protocols that are well suited to current experimental systems.

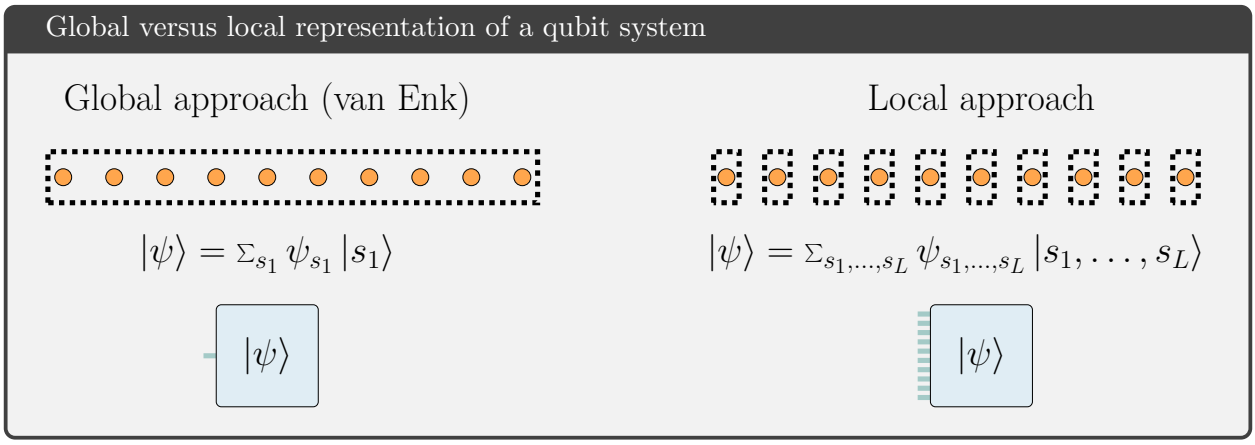

2.2 Graphical representation of quantum operations

Tensors representing quantum states can be easily transformed to describe physical processes.

First, a unitary operator U transforms quantum states into quantum states, and can be thus described by a $2N$ leg tensor. A initial state $|\psi\rangle$ is then transformed into a new state according to

$$U|\psi\rangle = \sum_{s_1,\ldots,s_N,s'_1,\ldots,s'_N} U_{s'_1,\ldots,s'_N,s_1,\ldots,s_N} \psi(s_1,\ldots,s_N) |s'_1\rangle \otimes \cdots \otimes |s'_N\rangle \tag{2.2}$$

Graphically these operations are obtained by linking the horizontal lines representing the indices from the two different tensors.

It is convenient to group indices that follow the same path into 'packed' indices, $(s_1, s_2, \ldots) \to s_X$, represented below as blue lines. For example, for defining a reduced density matrix ρ_A, we group the indices associated with A, and the complement B, and we trace out B by contracting its packed index s_B:

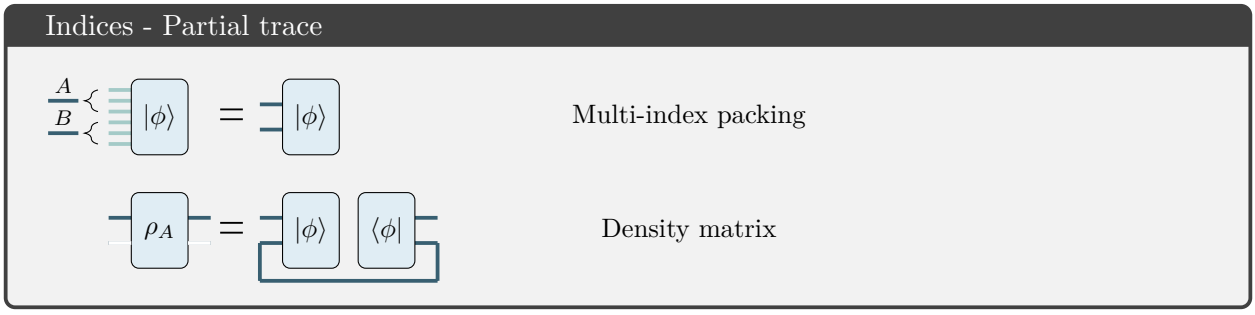

The density matrix ρ_A summarizes all the properties of the subsystem A. First, the expectation values of an observable O are obtained by the contraction of the density matrix with O. Some

physical quantities are not expectation values: One such quantity that is relevant for us is the purity $\mathrm{Tr}(\rho_A^2)$. In the following, we will omit the index A when there is no ambiguity.

Physical properties

$\langle O \rangle$ = 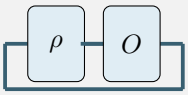

Expectation value

$\mathrm{Tr}(\rho^2)$ = 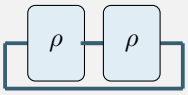

Purity

Measurement data is typically represented in the form of probabilities describing the state in a 'computational' basis $\{s\}$. This means that for a decomposition of the wavefunction with indices $s_1, \ldots, s_N$, the experiment provides us with an estimation of the probabilities $P(s) = \langle s | \rho | s \rangle$, with $|s\rangle = |s_1\rangle \otimes \cdots \otimes |s_N\rangle$ (corresponding to measuring the observables $O = |s\rangle \langle s|$). For a qubit system, $P(s)$ corresponds to a bitstring distribution. For an ultracold atom experiment with atoms loaded on L sites, $P(s)$ represents the population distribution of the atoms w.r.t each site, as measured by a quantum gas microscope (sometimes called 'full-counting statistics').

Measurement

$P(s)$ = 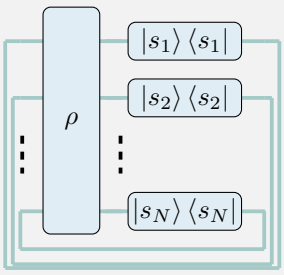

Fixed-Basis measurement

$P(s)$ = 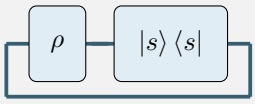

Fixed-Basis measurement
(indices packed)

Note that in the second line, we have written the same expression with packed indices, which obviously makes our life easier and improves the readibility of our diagrams.

The probabilities $P(s)$ are useful to measure expectation values of observables that are diagonal in the computational basis. For example, in a qubit system, one has access to spin correlations $\langle \sigma_i^z \sigma_j^z \rangle = \sum_s P(s) \sigma_i^z(s) \sigma_j^z(s)$ from bitstring measurements. Similarly, one can extract density-density correlations $\langle n_i n_j \rangle$ from population measurements in ultra-cold atoms setups that are equipped with a quantum gas microscope. For observables that are not diagonal in the computational basis, one can perform a unitary transformation prior to measurement, and effectively achieves a projective measurement in a different basis. For example with qubits systems, one can measure correlations $\langle \sigma_i^x \sigma_j^x \rangle$ in the x-basis via a Hadamard transformation occuring prior to the measurement. In the same spirit, the idea of randomized measurements is to perform *random*

operations before the measurements.

2.3 Introducting randomized measurements

How to measure quantities that are not associated with an observable, such as the purity? The idea of randomized measurements is to apply random unitaries

$$u = u_1 \otimes \cdots \otimes u_N \tag{2.3}$$

before the measurement, i.e each entity i is subject to a local random operation u_i. In particular, for qubit systems, this corresponds to applying random rotations u_i to each qubit independently, and measure the probabilities $P_u(s) = \langle s| u\rho u^\dagger |s\rangle = \mathrm{tr}(\rho\, u^\dagger |s\rangle \langle s| u)$.

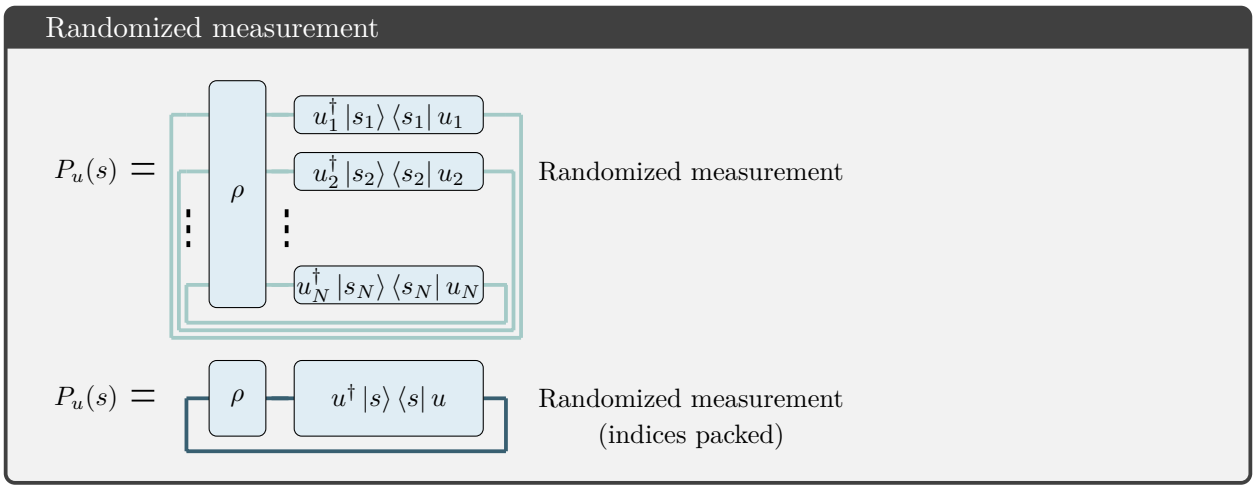

Van Enk and Beenakker [44] introduced the concept of randomized measurements for a single global constituent $N = 1$, and consider random unitaries from the circular unitary ensemble (CUE): This means that the unitaries u_1 are sampled according to the Haar measure on the unitary group $U(d)$ [54]. There exists numerical algorithms to generate random matrices from the CUE, e.g., using the QR decomposition [55]. However, as the physical implementation of a random unitary from the CUE requires exponential resources for quantum systems with local interactions [56], one can also consider for randomized measurements a different random ensemble of unitaries, *the unitary* $2-$*design* [57].

A unitary $2-$design $\mathcal{E}(2)$ produces the same ensemble averages as the CUE at the level of second order correlations, while its generation in an experiment would only require a polynomial number of local operations [56]. Mathematically, this statement reads

$$\int_{\mathcal{E}(2)} [u^{\otimes 2}] \otimes [(u^\dagger)^{\otimes 2}] du = \int_{\mathrm{CUE}} [u^{\otimes 2}] \otimes [(u^\dagger)^{\otimes 2}] du. \tag{2.4}$$

Note that, by definition, the CUE is a unitary $2-$design. For the general situation of arbitrary number of entities N considered here, we assume that each unitary u_i is sampled independently from a unitary $2-$design.

The magic of randomized measurements occurs when one starts correlating the results of two randomized measurements and calculate ensemble averages. Here, we rely on the following prop-

erties of unitary 2−designs [58]

$$\begin{aligned}\overline{(u_i)_{s_i,s_i^{(1)}}(u_i)^*_{s_i,s_i^{(2)}}} &= \frac{\delta_{s_i^{(1)},s_i^{(2)}}}{d}\\ \overline{(u_i)_{s_i,s_i^{(1)}}(u_i)^*_{s_i,s_i^{(2)}}(u_i)_{s_i,s_i^{(3)}}(u_i^*)_{s_i,s_i^{(4)}}} &= \frac{\delta_{s_i^{(1)},s_i^{(2)}}\delta_{s_i^{(3)},s_i^{(4)}}+\delta_{s_i^{(1)},s_i^{(4)}}\delta_{s_i^{(3)},s_i^{(2)}}}{d(d+1)},\end{aligned} \tag{2.5}$$

where δ is the Kronecker function, and $\overline{\bullet}$ is the ensemble average $\int_{\mathcal{E}(2)} \bullet\, du_i$. In order to understand these equations, let us consider the large $d \gg 1$ limit. In this case, we can assume in first approximation that each matrix element of u_i is taken independently from a normal distribution distribution of variance $1/d$ [44]. This allows us to understand the first line of Eq. (2.5), while the second line follows from the same logic. Note however the factor $d(d+1)$ (instead of d^2 for a normal distribution of variance $1/d$), which results from the fact that, due to the unitary constraint, the matrix elements of u_i are not completely independent, in particular for small values of d.

It is convenient for what follows to use ket and bra notations, $u_i = \sum_{s_i,s_i'} u_{s_i',s_i} |s_i'\rangle\langle s_i|$, and to combine Eqs. (2.5) to form a single equation

$$\overline{\langle s_i^{(2)}|\, u_i^\dagger\, |s_i\rangle\langle s_i|\, u_i\, |s_i^{(1)}\rangle\langle s_i^{(4)}|\, u_i^\dagger O_i(s_i) u_i\, |s_i^{(3)}\rangle} = \delta_{s_i^{(1)},s_i^{(4)}}\delta_{s_i^{(2)},s_i^{(3)}}, \tag{2.6}$$

where $O_i(s_i) = d(d+1)\,|s_i\rangle\langle s_i| - dI_i$ is a diagonal observable. This expression is better appreciated graphically, and is the mathematical backbone of randomized measurements. Equation (2.6) straightforwardly generalizes to several indices, subject to independent random unitaries u_i, as shown with the two last lines of the graphics below. Here $O(s) = O_1(s_1)\otimes\cdots\otimes O_N(s_N)$, and $u = u_1\otimes\ldots u_N$. In the graphics, we will always assume that the ensemble average over random unitaries is taken, without writing the overbar.

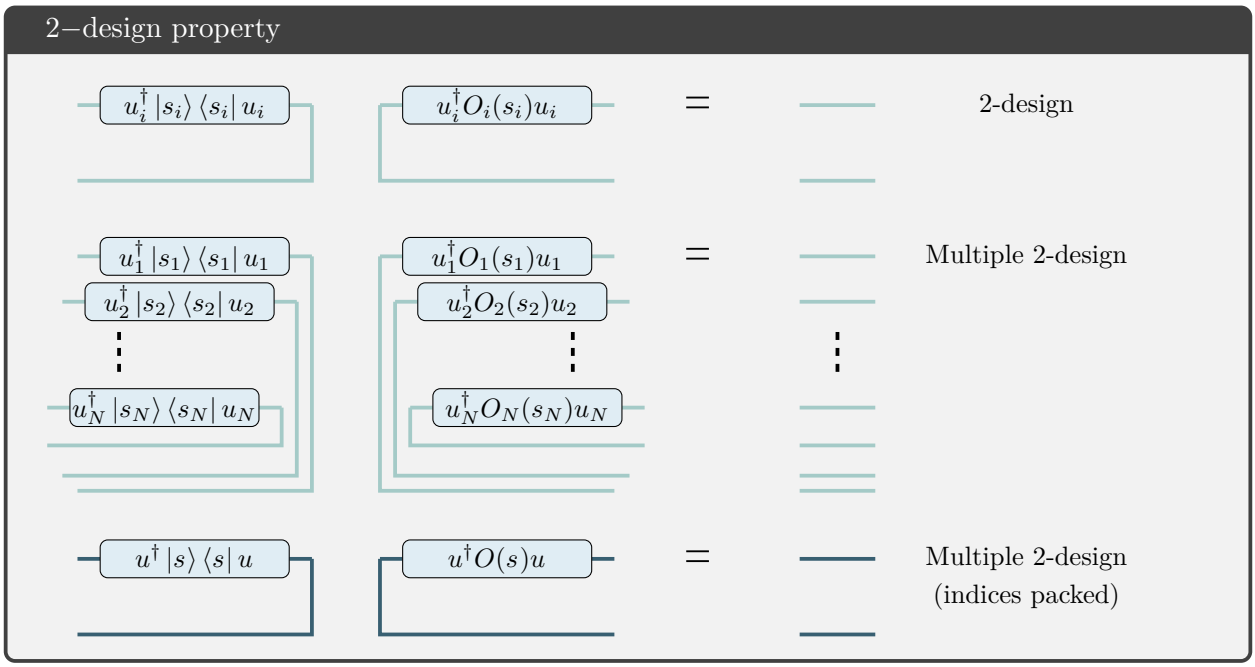

2.4 Second Rényi entropy from randomized measurements

We have introduced the mathematical tools to introduce our protocols. The general procedure to obtain a protocol consists in rewriting the quantity to be measured in terms of statistical correlations of randomized measurements (which can be measured). Graphically, this simply consists in cutting two horizontal lines, in order to insert the graphical 2−design identities written above. The location of this cut-glue surgery is shown below as a rectangle with dashed lines. For the purity, we obtain

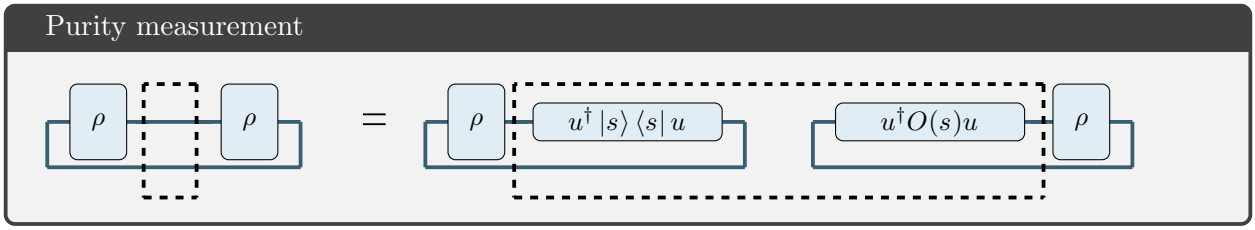

In a graphical way, we have proven our first result on randomized measurement [45, 47]

$$\mathrm{tr}(\rho^2) = \overline{P_u(s)\mathrm{tr}(u\rho u^\dagger O(s))}. \tag{2.7}$$

Using

$$\begin{aligned} O(s) &= \bigotimes_i (d(d+1)\,|s_i\rangle\langle s_i| - dI_i) = d^{2N} \bigotimes_i \left(|s_i\rangle\langle s_i| - \frac{1}{d}\sum_{s_i' \neq s_i} |s_i'\rangle\langle s_i'| \right) \\ &= d^{2N} \bigotimes_i \left(\sum_{s_i'} (-d)^{-D[s_i,s_i']}\, |s_i'\rangle\langle s_i'| \right) = d^{2N} \sum_{s'} (-d)^{-D[s,s']}\, |s'\rangle\langle s'|\,, \end{aligned} \tag{2.8}$$

where $D[s,s'] = \sum_i (1-\delta_{s_i,s_i'})$ is a coefficient, which reduces to the familiar Hamming distance in the qubit case $d=2$, this result can be written as

$$\mathrm{tr}(\rho^2) = d^{2N} \sum_{s'} (-d)^{-D[s,s']} \overline{P_u(s)P_u(s')}. \tag{2.9}$$

We can finally average this equation over all basis s states, and obtain the final expression of the purity

$$\mathrm{tr}(\rho^2) = d^{N} \sum_{s,s'} (-d)^{-D[s,s']} \overline{P_u(s)P_u(s')}, \tag{2.10}$$

and of the second Rényi entropy

$$S_2(\rho) = -\log\left(d^{N} \sum_{s,s'} (-d)^{-D[s,s']} \overline{P_u(s)P_u(s')} \right). \tag{2.11}$$

Our expressions have been derived in full generality for a system of N entities in Refs [45] (in a different form) and in Refs. [43, 47]. In the limiting case $N=1$, we can rewrite Eq. (2.10) as

$$\mathrm{tr}(\rho^2) = d \sum_s \overline{P_u(s)^2} - \sum_{s\neq s'} \overline{P_u(s)P_u(s')} = (d+1)\sum_s \overline{P_u(s)^2} - 1, \tag{2.12}$$

i.e., we recover the original result from van Enk and Beenakker [44], Eq.(1.17).

Our motivation to derive the multi-entity approach $N > 1$ [45, 43, 47] was to drastically simplify the experimental task by replacing global unitaries by local ones for qubit systems. Indeed, consider N qubits with $d = 2$, the protocol consists in applying random single qubit rotations u_i on each qubit independently, which is a task that can be realized in various experiments with very high fidelity.

2.5 Experimental demonstration of randomized measurements

Randomized measurements were first demonstrated in a qubit system of $L = 10$ ions [43]. The reduced purities of the many-body quantum state were obtained with randomized measurements based on local random unitaries, which corresponds to the protocol described above with number of entities $N = L = 10$, and local Hilbert space dimension $d = 2$.

2.5.1 System and Hamiltonian

In our trapped ion quantum simulator, a set of L Calcium ions was trapped via electrodes in a Paul trap configuration [59]. Due to the Coulomb interactions, these ions typically align in a quasi one-dimensional crystal geometry. As thermal phonon excitations are very efficiently suppressed via laser-cooling, the system can be described in terms of a qubit system. The qubits are encoded in two long-lived electronic states of each ion, with such two states separated by a dipole-forbidden transition. An image of a 20-ion string is shown in Fig. 2.1

The trapped ion quantum technology is based on making the qubits interact via virtual phonon excitations. To do so, a laser field is shined on the ions so that, due to an off-resonant light-matter coupling, a change of electronic level in one qubit can result in the creation of a phonon excitation [59]. This phonon propagates in the ion chain and can be finally absorbed by a second qubit. In the so-called Lamb-Dicke regime, the phonon degree of freedom can be eliminated perturbatively, and we can describe the coupling between the qubits by an effective Hamiltonian

$$H_{XY} = \sum_{i<j} J_{ij}(\sigma_i^+ \sigma_j^- + \text{h.c.}), \tag{2.13}$$

with power law interactions $J_{ij} \sim J/|i-j|^\alpha$, $0 < \alpha < 3$. Effectively, the phonon modes thus generate a coherent dipolar exchange interactions between the qubits. Note that the very same mechanism can be used to generate two-qubit gates, such as the Cirac-Zoller gate or the Mølmer-Sørensen gate, which are the basis of trapped ion quantum computers [59].

2.5.2 Generation of an entangled state

In addition to the coupling term H_{XY} that can be switched on and off, the state of each qubit can be manipulated locally to prepare any product state $|\psi_0\rangle$. The same quantum 'hardware' can be used to generate arbitrary local rotations $u = u_1 \otimes \cdots \otimes u_N$ for randomized measurements.

In the present case, the system was initialized in the Néel state $|\psi_0\rangle = |0, 1, 0, 1, \ldots\rangle$, and then was time-evolved via the Hamiltonian Eq. (2.13), in order to produce an entangled state

$$|\psi(t)\rangle = \exp(-iH_{XY}t)\,|\psi_0\rangle\,. \tag{2.14}$$

This situation represents the paradigmatic situation of thermalization [36]. Initially, the entanglement entropy of any subystem is approximately zero $S_2(\rho_A) \sim 0$. As time evolves, the entropy of subsystems will increase progressively as the result of thermalization, while the entropy of the total system will remain approximately zero during such a unitary process.

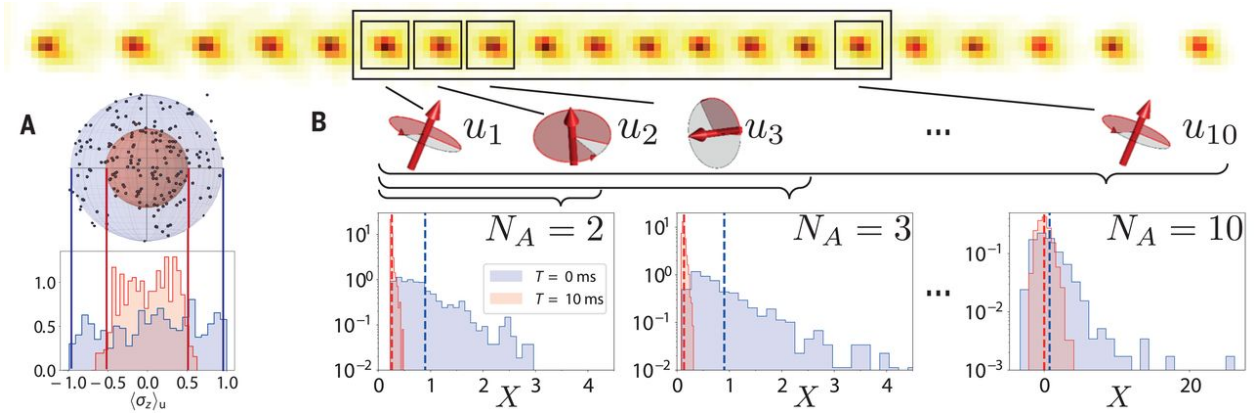

Figure 2.1: Randomized measurement protocols implemented in a trapped ion quantum simulator [43].

2.5.3 Randomized measurements

In order to measure entanglement after a certain evolution time, the coupling lasers are switched off and the randomized measurements sequence starts. At this point, random 2×2 unitaries from the CUE generated numerically [55] are converted, via standard trigonometry, to a sequence of qubits rotations R_i^z, R_i^x along the z and x axes

$$u_i = R_i^x(-\pi/2)R_i^z(\theta_{i,1})R_i^x(\pi/2)R_i^z(\theta_{i,2}). \tag{2.15}$$

This decomposition offers the advantage of requiring only local addressing on the z axis, while the ions can be rotated simultaneously along the x-axis via a global beam[1].

After application of a given random unitary u, a bitstring s was collected by projective measurement implemented by single site resolved fluorescence imaging [59]. This sequence was repeated $N_M = 150$ times to obtain an estimation of the randomized measurement probabilities $P_u(s)$. This procedure was repeated for $N_u = 500$ unitaries, corresponding to a total of 500×150 repetitions of the experiment. Based on this data, we could obtain estimates of the purity $\mathrm{tr}(\rho_A^2)$ for all possible 1024 subsystems ρ_A of the 10 ion system via Eq. (2.10).

2.5.4 Results

The results of this experiment are shown in Fig. 2.2. At time $t = 0$, the purity is close to unity for all shown subsystems, showing that we indeed managed to prepare with high fidelity a pure product state $|\psi_0\rangle$. As entanglement is generated by time evolution, the purities of the subsystems decrease with time, while the entanglement entropies increase. In contrast, the purity and entropy of the total system stay at their initial values, showing that the system undergoes unitary dynamics. In particular, for the late times, we can use the criterion Eq. (1.9) and detect entanglement for all 1024 bipartitions of the system, see panel (C).

These results constitute the first direct measurements of entanglement entropies in a single quantum system. Moreover, this demonstration with 10 ions corresponds to a situation that is beyond the regime of applicability of state-tomography. In conclusion, we could show in this experiment the potential of randomized measurements to become a method of reference for probing entanglement in many-body quantum systems.

[1] To optimize the randomness of the random unitaries, two unitaries of the form above were actually concatenated in the experiment.

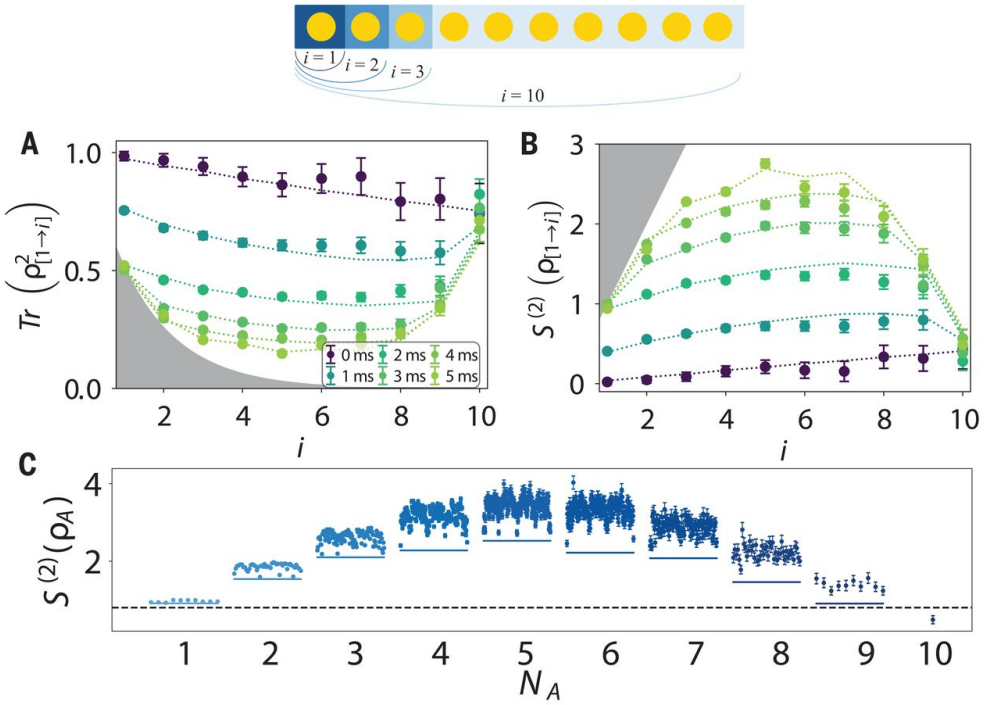

Figure 2.2: Measurement of Rényi entanglement entropies [43]. Estimation of the purities (A) and of the second Rényi entropies (B) for connected partitions of the type $A = \{1, \ldots, i\}$. In panel (C), we represent $S^{(2)}(\rho_A)$ for all 1024 bipartitions at $t = 5$ ms.

2.6 Measurement of entanglement entropies with global random unitaries

In non-qubit systems, randomized measurements can also be realized using the global approach $N = 1$ [44]. In the present section, we review our work [45, 46] showing how to physically realize the required global random unitaries from a 2−design in quantum simulators.

Consider for concreteness a one-dimensional Fermi-Hubbard (FH) model of L sites (here $\hbar = 1$)

$$H_{FH} = -J \sum_{i=1}^{L-1} \sum_{\sigma} c_{i,\sigma}^{\dagger} c_{i+1,\sigma} + U_{\text{int}} \sum_{i=1}^{L} n_{i,\uparrow} n_{i,\downarrow}. \tag{2.16}$$

Here $c_{i,\sigma}$ annihilates a fermion of spin σ ($\sigma = \uparrow, \downarrow$) at site i, and $n_{i,\sigma} = c_{i,\sigma}^{\dagger} c_{i,\sigma}$ is the local fermion density. The Fermi-Hubbard model plays an important role in quantum simulation: It has been introduced to model the behavior of strongly correlated electronic systems in the context of high-temperature superconductivity, and can be realized with ultracold atoms loaded in optical lattices [1].

In order to access the entanglement properties of the FH model via randomized measurements, one has to realize global random unitaries acting on the entire partition ρ_A of interest[2]. How to *physically generate* the required global random unitaries u from a 2−design? In Refs [45, 46], we

[2]The system being subject to particle and spin conservation, it is not possible to use 'local' random unitaries on each lattice site independently.

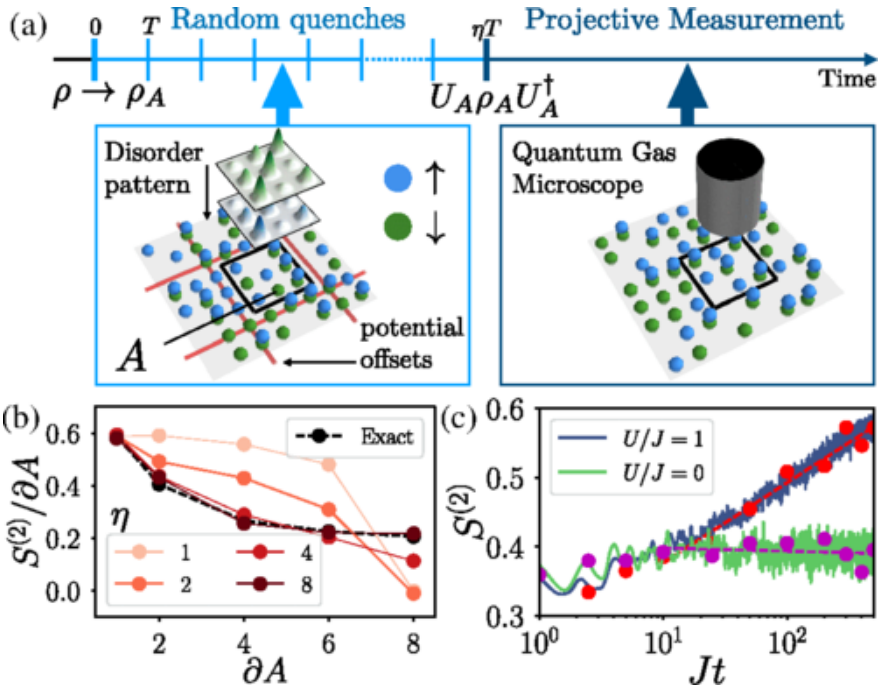

Figure 2.3: Generation of global random unitaries via random quenches [45] [(a)], and application to the measurement of the second Rényi entropy of the groundstate of the two-dimensional Heisenberg model [b)], and of a many-body localized phase in the Bose Hubbard model [c)].

propose to realize 'random quenches'

$$u = \prod_{j=1}^{\eta} \exp\left(-i\left[H_{FH|A} + \sum_{i\in A} \epsilon_{i,\sigma}^{(j)} n_{i,\sigma}\right] T\right), \tag{2.17}$$

where $H_{FH|A}$ is the Fermi-Hubbard model Eq. (2.16) restricted to A, T is a fixed evolution time, and $\epsilon_i^{(j)}$ is a disorder term. The proposed physical implementation of the unitary is depicted in Fig. 2.3 a). The partition of interest A is isolated using energy barriers, and a spin-dependent disorder potential is applied. This disorder is changed η times to generate η random quenches, as in Eq. (2.17). Note that unitaries of the type Eq. (2.17) have also been studied as candidates to generate unitary 2−designs in Refs [56, 60, 61].

For us, the key question to be addressed was: To which extent a distribution of random quenches, representing only an *approximate* 2−design, allow to measure purities and Rényi entropies via randomized measurements? In order to answer this question, we chose a set of 'test states' ρ_A and compare the purity $\mathrm{tr}(\rho_A^2)$ with the estimation obtained via the formula Eq. (2.10). We performed this analyzis for the FH model, but also for the Bose-Hubbard model, and several spin models.

In Fig. 2.3a), we illustrate this procedure with the example of an area law that is satisfied by the ground state of a two-dimensional Heisenberg model. At small η, time evolution generated by the random quenches does not produce a sufficient amount of randomness for forming a 2−design. Therefore the estimated Rényi entropy is a very bad approximation of the exact value (dashed line). At larger η, convergence to a 2−design is achieved and we obtain a faithful estimation of $S_2(\rho_A)$. The protocol can also be applied to study non-equilibrium dynamics, see Fig. 2.3b).

How does the time $t = \eta T$ needed to create an approximate 2−design increase with system size L? For one-dimensional models, we have numerically observed that the required evolution

t only increases linearly with system size L, and is minimized when the disorder strength, the quench frequency T^{-1}, and the characteristic frequencies of the Hamiltonian (e.g., J and U_{int}) are all comparable. This is compatible with earlier results obtained for specific models [56, 60, 61], and shows that global random unitaries can be generated efficiently in quantum simulators implementing spin or Hubbard models, and used to faithfully measure purities and entanglement entropies.

2.7 Statistical errors and imperfections

Finally, we conclude this chapter by addressing the role of statistical and systematic errors. The statements, which we make here in the context of the measurement of the purity, also apply to the other quantities that we can measure with randomized measurements, see below.

2.7.1 Statistical errors

In an experiment, the purity of a quantum state ρ is estimated via Eq. (2.10) with an ensemble average over a *finite* number of unitaries N_u, and with probabilities $P_u(s)$ estimated from a *finite* number of measurements N_M (per unitary). To understand the role of statistical errors originated from the finite values of N_u and N_M, let us first present the details of the postprocessing of experimental data. We will then give simple estimates for the scaling of statistical errors, which we can also compare with numerical simulations.

Post-processing the experimental data

In order to obtain an estimation of the purity from 'raw' experimental data, one proceeds as follows. For each random unitary u_r ($r = 1, \dots, N_u$), one acquires N_M projective measurements in a fixed basis $\{s\}$, which we label $s_{r,m}$ ($m = 1, \dots, N_M$) (recall for example that $s_{r,m}$ correspond to bitstrings for a qubit system). Each measurement $s_{r,m}$ is a discrete random variable that is sampled according to a Bernoulli distribution with discrete probabilities $P_{u_r}(s)$. Therefore, we can build estimations of such probabilities by empirical averages

$$P_{u_r}^{(e)}(s) = \sum_{m=1}^{N_M} \frac{\delta_{s,s_{r,m}}}{N_M}, \tag{2.18}$$

Multiplying naively the estimates of the probability to obtain the purity via Eq. (2.10) would provide a biased estimation, i.e, a quantity whose average, in the sense over many repetitions of the protocol, would not be the exact purity. Instead, based on U-statistics [62], we can construct unbiased estimators for polynomials of the vector $P_{u_r}(s)$ simply by using different projective measurements [45, 46]

$$[P_{u_r}(s)P_{u_r}(s')]^{(e)} = \sum_{m\neq m'} \frac{\delta_{s,s_{r,m}}\delta_{s',s_{r,m'}}}{N_M(N_M-1)}, \tag{2.19}$$

We can now use Eq. (2.10) and obtain our estimation of the purity

$$\begin{aligned}[\text{tr}(\rho^2)]^{(e)} &= \frac{d^N}{N_u}\sum_r\sum_{s,s'}(-d)^{-D[s,s']}[P_{u_r}(s)P_{u_r}(s')]^{(e)} \\ &= \frac{d^N}{N_uN_M(N_M-1)}\sum_r\sum_{m\neq m'}(-d)^{-D[s_{r,m},s_{r,m}]}.\end{aligned} \tag{2.20}$$

Eq. (2.20) illustrates that the estimation of the purity is provided by a bilinear operation on the measurement data $s_{r,m}$. Note that the data postprocessing task of randomized mesurements is therefore a simple task, which does not require large memory storage and can be also massively parallelized. Having in mind the classical optimization procedures needed for tomographic methods [3, 7], this represents a strong added value for randomized measurements. We provide in Ref. [63] an open-source repository, with a python code that can postprocess randomized measurements based on Eq. (2.20).

Scaling of statistical errors

Our estimation $[\mathrm{tr}(\rho^2)]^{(e)}$ is unbiased, i.e we measure in average the true value of the purity. However, the statistical error

$$\mathcal{E} = \mathrm{avg}[|\mathrm{tr}(\rho^2)]^{(e)} - \mathrm{tr}(\rho^2)|], \tag{2.21}$$

where avg represents an averaging over many repetitions of the protocol, takes a finite positive value. An important question to assess the feasibility of our protocol is therefore: What is the required value of N_M and N_u to ensure that the statistical error $\mathcal{E}$ is compatible with a given accuracy?

A simple estimation for statistical errors can be derived as follows for the case $N = 1$ [46]. The purity estimation has the form of an empiral average over random unitaries

$$\mathrm{tr}(\rho^2) = \frac{1}{N_u d} \sum_{r,s} A(r,s) \tag{2.22}$$

with $A(r,s) = d^2 P^2_{u_r}(s)$ (assuming the large d limit, $d+1 \approx d$). The average statistical error for $A(r,s)$ can be analytically estimated by calculating, using the statistics on Bernoulli distributions, the variance of $[P_{u_r}(s)^2]^{(e)}$, as given in Eq. (2.19). In the most relevant regime for randomized meaurements, $N_M \ll d$, we find $\mathcal{E}[A(r,s)] \sim d/N_M$ [64]. Assuming in first approximation that all terms $A(r,s)$ are independent, we obtain

$$\mathcal{E} \sim \frac{1}{\sqrt{N_u d}} \mathcal{E}[A(r,s)] = \frac{1}{\sqrt{N_u}} \left(\frac{\sqrt{d}}{N_M} \right). \tag{2.23}$$

In other words, in order to obtain an error of the order of $1/\sqrt{N_u}$, we require a number of projective measurements $N_M \sim \sqrt{d}$. It is surprising that the required number of measurements to estimate the purity is *smaller* than the Hilbert space dimension d, meaning that only few states are actually observed during the protocol. This is due to a well known statistical effect, the 'Birthday paradox'. The probability to observe twice the same state with N_M samples, which is the key 'statistical event' that controls the accuracy of purity estimation, c.f Eq. (2.20), indeed scales as the square root of the number of the possibilities d.

For $N = 1$, our estimate shows that the total number of measurements $N_u N_M$ to obtain a given accuracy scales as the Hilbert space dimension $\sqrt{d}$. For the protocol with qubits and local unitaries, we numerically observed that the error is more of the order of d^{aN}, $a \approx 1$ [43] (here the Hilbert space dimension becomes d^N). For both protocols, we thus note a remarquable advantage in terms of required measurements over state tomography, which requires approximately 4^N measurements [3]. In their current versions, randomized measurement protocols are expected to be applicable to partition sizes up to 20 qubits. For illustration, we show in Fig. 2.4 the scaling of the required value of $N_U N_M$ to measure the purity with relative error 0.12 for a qubit system of N_A sites and various quantum states.

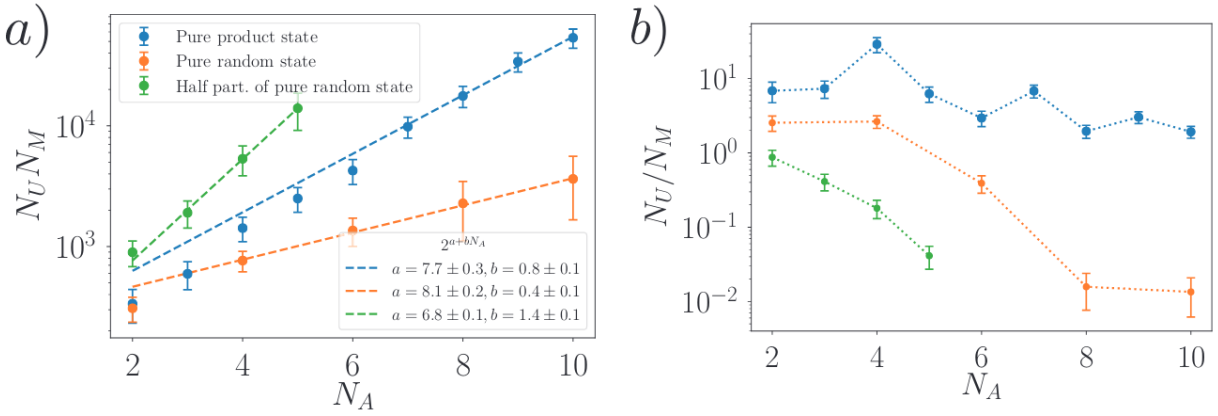

Figure 2.4: a) Scaling of the total number of measurements $N_u N_M$ to obtain a given accuracy, and b) optimal ratio minimizing the statistical error for a given value of $N_u N_M$ [43].

Finally, for a fixed measurement 'budget' $N_u N_M$, the question of how one should choose the value of N_u and N_M to minimize statistical errors is also of practical interest. As shown in Fig. 2.4 b), the optimal ratio N_u/N_M depends on the quantum state (a priori unknown) being probed. We discuss at the end of this manuscript strategies for reducing statistical errors via importance sampling of random unitaries.

2.7.2 Imperfections

We now discuss the role of systematic errors in randomized measurements protocols.

Miscalibration

For concreteness, let us address the problem of miscalibration for our protocol with local random unitaries in a qubit system. In this case, the random unitaries u_i are qubit rotations, which can be parametrized as in Eq. (2.15). Due to an imperfect calibration of the experiment, the unitaries $\tilde{u}_i$ that are physically realized can differ from the unitaries u_i that we expected to generate (this is sometimes called a 'unitary error').

Randomized measurements have robustness properties against miscalibration. Suppose for simplicity that we can write $\tilde{u}_i = u_i v_i$, where u_i is picked from the CUE, and v_i is an unwanted fixed rotation. In this case, the purity estimation will not be affected, because, according to the Haar measure, if u_i is sampled from the CUE, $u_i v_i = \tilde{u}_i$ is also sampled from the CUE [54]. In brief, a random unitary multiplied by another unitary is still a random unitary that can be used for our protocols.

Decoherence

In contrast to miscalibration, decoherence can affect the estimation of the purity. Decoherence can be due for example to spontaneous emission, or to errors in measurement readout [59].

Here, for concreteness we consider that the state is depolarized due to decoherence

$$\rho_u = (1-p) u \rho u^\dagger + \frac{p}{d}\mathbf{1}, \tag{2.24}$$

where $\mathbf{1}$ is the $d \times d$ identity matrix, and $0 < p < 1$ is the strength of the noise. The depolarization noise term commutes with any unitary operation, i.e., we can write ρ_u as

$$\rho_u = u\rho_p u^\dagger, \tag{2.25}$$

with $\rho_p = (1-p)\rho + (p/d)\mathbf{1}$. This means that we can imagine that decoherence had indeed occured *before* randomized measurements were performed. Randomized measurements being performed in this picture on ρ_P, we obtain an estimate

$$\mathrm{tr}(\rho_p^2) = (1-p)^2 \mathrm{tr}(\rho^2) + \frac{p(2-p)}{d}. \tag{2.26}$$

Decoherence thus leads to an underestimation of the purity. We have studied this effect for various decoherence models in Refs. [46]. In the context of the experimental demonstration of randomized measurements [43], the loss of purity for each qubit was of the order of 1%.

Chapter 3

The randomized measurement toolbox

We have introduced in the previous chapter the general ideas behind randomized measurements in the context of the purity measurement. In the present chapter, we review the works [48, 49, 50, 65], where we derived and experimentally demonstrated protocols to measure other quantities associated with many-body entanglement.

In order to derive the formulas that map the quantities to be measured to statistical correlations of randomized measurements, we will take advantage of the graphical approach that was developed in the previous chapter.

3.1 Measuring out-of-time-order correlations

Out-of-time-order correlations (OTOCs) have been recently studied in the context of quantum chaos in high-energy physics [66, 67]. The idea is to consider a Hermitian operator W that is evolved via a unitary operation $U(t)$ according to the Heisenberg picture $W(t) = U(t)^\dagger W U(t)$. The OTOC is defined as

$$\tilde{O}(t) = \frac{\mathrm{tr}(\rho_0 W(t) V W(t) V)}{\mathrm{tr}(\rho_0 W^2(t) V^2)}, \tag{3.1}$$

where ρ_0 is a density matrix, and V is an operator, which is here assumed Hermitian and unitary, and which commutes with the initial value of the W operator, i.e., $[W(0), V] = 0$. The OTOC can be simply related to the norm of the commutator between the operators $W(t)$ and V [67]. In particular, the OTOC is initially unity, $\tilde{O}(t = 0) = 1$, and will then generically decay as a function of time, as the two operators $W(t)$ and V start overlapping.

The decay of the OTOC as a function of time has been recognized as a signature of quantum chaos. In certain models of high-energy physics that are relevant to describe quantum dynamics at the horizon of a black-hole, such as the Sachdev-Ye-Kitaev (SYK) model [68, 69], the decay of OTOCs is in particular exponential, which is conjectured to be a signature of 'fast scrambling' [70]. This means that information that is initially encoded locally (which could be 'revealed' by a local measurement $W(0)$) becomes after time evolution quickly delocalized (or 'scrambled') and therefore no longer accessible to local measurements [67]. Inspired by these theoretical developments, the study of OTOCs has been recently extended to condensed matter, revealing universal aspects of thermalization dynamics [71, 72, 73, 74, 75, 76]. There is thus a growing interest in measuring OTOCs in quantum simulators and quantum computers.

Unfortunately, for an experimentalist, measuring OTOCs is not as easy as measuring a standard correlation function, the reason being the 'out-of-time' ordering that is apparent in Eq. (3.1). The first experimental measurements of OTOCs could only be realized recently in a spin system with

infinite range interactions [77], or with a 'small' 4-qubit quantum computer [78]. In these experiments, OTOCs could be measured by reversing the sign of the Hamiltonian $H \to -H$ during time evolution, in order to reproduce the time-ordering sequence of Eq. (3.1), and following the protocols developed in Refs. [79, 80, 81]. For generic experimental platforms, implementing kinetic energy terms, local interactions, etc, changing dynamically the sign of the Hamiltonian is an outstanding challenge. This motivates new approaches to measure OTOCs.

Randomized meausurements protocols allow us to measure OTOCs without reversing the sign of the Hamiltonian during time evolution, and are thus applicable to generic physical setups. In the following, we present our theory protocol [48], as well as the experimental demonstration with a 10-qubit trapped ion quantum simulator [49].

3.1.1 Randomized measurement protocol

In the case of the purity measurement, statistical correlations were used to decompose a non-linear function into a product of observables (the randomized measurements). Here, we use the same trick to decompose an out-of-time order correlation function into a product of two correlation functions, which can be both measured separately. Graphically, this reads

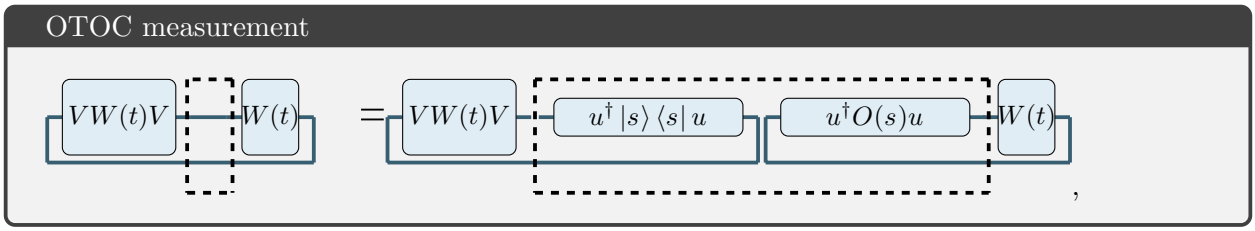

with the same notations as in chapter 2. Replacing $O(s)$ by its definition, we obtain

$$\mathrm{Tr}(VW(t)VW(t)) = \sum_{s'} (-d)^{D[s,s']} \overline{\langle VW(t)V\rangle_{u,s} \langle W(t)\rangle_{u,s'}} \tag{3.2}$$

with $\langle W(t)\rangle_{u,s'} = \langle s'| uW(t)u^\dagger |s'\rangle$, and $\langle VW(t)V\rangle_{u,s} = \langle s| VuW(t)Vu^\dagger |s\rangle$, which are standard, easily measurable, *time-ordered* correlation functions. This equality in turn implies that we can measure the infinite temperature OTOC, $\rho_0 = \mathbf{1}/d^N$ as

$$\tilde{O}(t) = \frac{\sum_{s'} (-d)^{-D[s,s']} \overline{\langle VW(t)V\rangle_{u,s} \langle W(t)\rangle_{u,s'}}}{\sum_{s'} (-d)^{-D[s,s']} \overline{\langle W(t)\rangle_{u,s} \langle W(t)\rangle_{u,s'}}}. \tag{3.3}$$

The protocol for measuring OTOCs via randomized measurements based on Eq. (3.3) is illustrated for a L-qubit system in Fig. 3.1 for both global random unitaries ($N = 1$, $d = 2^L$) and local random unitaries ($N = L$, $d = 2$). There are two types of experiments to be performed. (i) First, one applies a random unitary $u^\dagger$ (or equivalently u, as in the figure) on an initial state $|s'\rangle$, which is then time-evolved with the Hamiltonian. After that, the operator W is measured, providing us with an expectation of $\langle W(t)\rangle_{u,s}$. (ii) The second type of experiment is identical to the first one, except that V is applied before time evolution, and we obtain $\langle VW(t)V\rangle_{u,s}$. According to Eq. (3.3), the OTOC $\tilde{O}(t)$ is extracted from the statistical correlations between the two measurements.

3.1.2 Sampling of initial states

Equation (3.3) suggests that one must use all basis states $|s'\rangle$ as initial states to access the infinite temperature OTOC, a daunting task for a many-body system with an exponentially large Hilbert

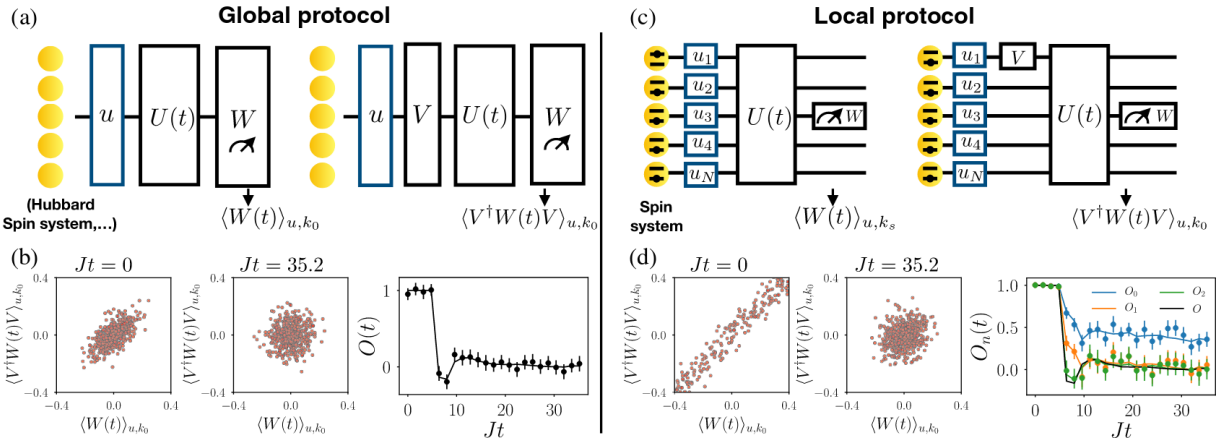

Figure 3.1: Randomized measurement protocol for OTOCs [48]. Either with global [(a)] and local [(b)] random unitaries, a random initial state is created and time-evolved with the operator U. Statistical correlations between randomized measurements of the operator W reveal the OTOC.

space. Fortunately, we can simplify our protocol, and use in fact a very restricted number of initial states.

First, for global unitaries, $N = 1$, only one initial state $|s\rangle$ is sufficient to measure $\tilde{O}(t)$, as we can write

$$\begin{aligned}\sum_{s'}(-d)^{-D[s,s']}\langle VW(t)V\rangle_{u,s}\langle W(t)\rangle_{u,s'} &= \langle VW(t)V\rangle_{u,s}\left(\langle W(t)\rangle_{u,s}-\frac{1}{d}\sum_{s'\neq s}\langle W(t)\rangle_{u,s'}\right)\\ &= \left(1+\frac{1}{d}\right)\langle VW(t)V\rangle_{u,s}\langle W(t)\rangle_{u,s},\end{aligned} \tag{3.4}$$

where we have assumed that $\mathrm{tr}(W(t)) = \mathrm{tr}(W) = 0$ (without loss of generality, as one can always redefine the Hermitian operator $W \to W - \mathrm{tr}(W)$).

In the general case $N \geq 1$, such a drastic simplication is not possible. However, we can use a restricted number of initial states and obtain faithful estimations for the OTOCs. For the qubit case ($d = 2$), we have introduced the modified OTOCs

$$\tilde{O}_n(t) = \frac{\sum_{s'\in E_n}(-2)^{-D[s,s']}\overline{\langle VW(t)V\rangle_{u,s}\langle W(t)\rangle_{u,s'}}}{\sum_{s'\in E_n}(-2)^{-D[s,s']}\overline{\langle W(t)\rangle_{u,s}\langle W(t)\rangle_{u,s'}}}, \tag{3.5}$$

where the ensemble E_n ($n = 0, \ldots, N$) denotes the set of 2^n basis states $\{s'\} = \{s'_1, \ldots, s'_L\}$, such that only the first n qubits differ from our reference state $|s\rangle$, i.e., $s'_i = s_i$, for $i > n$.

Obviously, the series of modified OTOCs converges to the OTOCs at $n = N$, i.e., $\tilde{O}_N(t) = \tilde{O}(t)$. The good news is that the low order terms $n = 0, 1, \ldots,$ generically already give good approximations of the OTOC [48], see for instance Fig. 3.1 for an example with the Kicked Ising model. Having a fast converging series of modified OTOCs implies, that in an experiment, one can access OTOCs based on preparing only a small number of initial states. For example, for measuring $\tilde{O}_2$, we only need $2^2 = 4$ initial states.

3.1.3 Experimental observations

Our protocol was first experimentally demonstrated with a 4 qubit quantum computer based on nuclear magnetic resonance (NMR) [82]. The authors used global random unitaries, confirming earlier experimental results obtained with changing the sign of the Hamiltonian [78]. In our work [49], we took advantage of our protocol to study the 'scrambling' of quantum information in a large many-body system with local interactions, i.e., in a situation where OTOCs could not be measured so far. In our case, we used local random unitaries.

As for the Rényi entropy measurement [43], the system under study was a 10-qubit trapped ion quantum simulator, subject to the long-range XY-model Eq. (2.13). Based on numerical simulations, we checked that the second modified OTOC $O_2(t)$ is a good approximation of the exact OTOC $O(t)$, meaning that only four initial states $|s'\rangle$ were needed, see Fig. 3.2.

Randomized measurements were performed by preparing initial random product states and letting the system evolve until a time t, when a measurement of the operators $W = \sigma_j^x$, $j = 1, \ldots, N$ was performed. The operator V was fixed to $V = \sigma_1^z$. We show in Fig. 3.2 the results of the measurements for two values of the interaction power-law exponent α. For $\alpha = 1.22$, the measurements are compatible with the existence of a 'butterfly velocity' v_B [75, 76], as the characteristic time of decay $t_c \propto j/v_B$ of the OTOC approximately increases linearly with the position j of the W operator. Instead, for longer range interactions, $\alpha = 0.85$, we noticed that the space-time profile of the OTOCs cannot be linked to the existence of a butterfly velocity.

Our protocol has enabled the observation of quantum information scrambling in a many-body system, and put into evidence the crucial role of long-range interactions. This may open up interesting possibilities to probe scrambling in situations that are relevant to the scenario of fast-scrambling, e.g by measuring OTOCs in the Sachdev-Ye-Kitaev (SYK) model [68, 69].

3.2 Cross-platform verification of quantum devices

Rényi entropies or OTOCs are useful to probe the many body properties of a quantum system. But how to verify that the quantum state that is prepared in an experiment is really the state that we expected to prepare? Our work [65] extends the use of randomized measurements to measure state fidelities.

Our strategy to verify the quality of preparation of a quantum state consists in measuring the fidelity between two different density matrices ρ_1, and ρ_2. We can first consider the situation of *theory-experiment verification*, where the first quantum state ρ_1 is physically realized in an experiment, e.g. a trapped ion quantum simulator, and the second state ρ_2 is a theory representation of the state on a classical computer, i.e., obtained by a numerical simulation. In the regime of quantum advantage, such theory-experiment verification cannot be realized, as it is not possible to represent the state ρ_2 on a classical computer. However, we can perform *experiment-experiment (or 'cross-platform') verification*, comparing two states ρ_1 and ρ_2 that are realized in two different experiments. These two experiments are designed to ideally create the same state ρ so that, when the two states significantly differ, we can conclude that at least one quantum device suffers from errors. If instead the two devices are shown to produce the same quantum state, $\rho_1 \approx \rho_2$, one can gain confidence in the fact that both devices operate as expected.

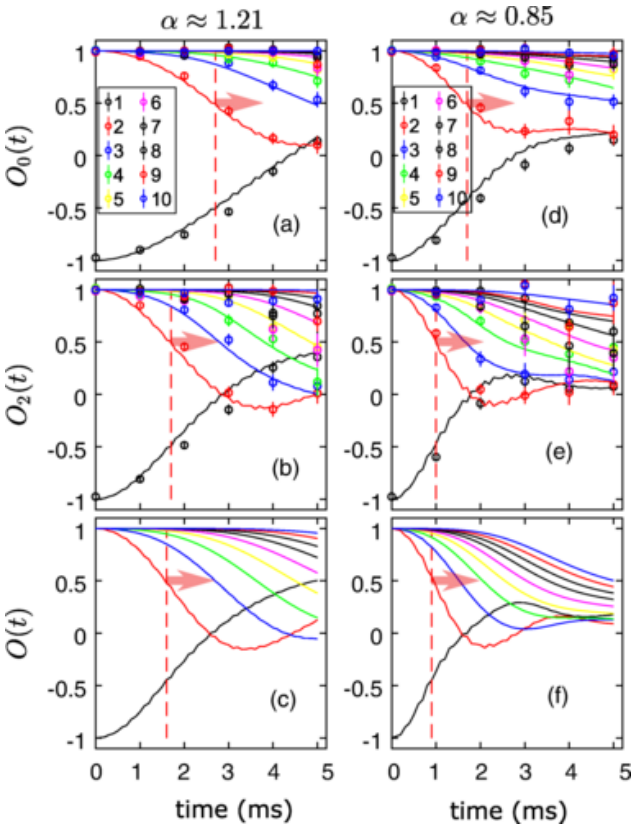

Figure 3.2: OTOC measurements in a trapped ion system [49]. The modified OTOCs $O_{0,1,2}(t)$ were measured using randomized measurements obtained from four different initial states. The dots correspond to the experimental measurements, while solid lines represent numerical simulations.

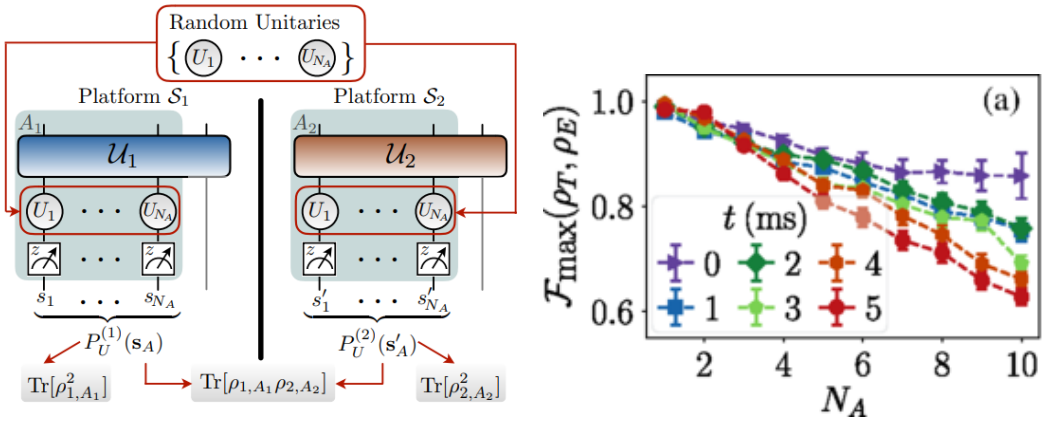

Figure 3.3: Randomized measurements of Measurement of fidelities between a experimental and a theory state [65], based on the randomized measurement data produced for Ref. [43].

3.2.1 Introducing quantum state fidelities

There exists various fidelity meaures to quantify the overlap between two quantum states. Here, we will be interested in the 'max' fidelity [83]

$$F_{\max}(\rho_1,\rho_2) \quad = \quad \frac{\mathrm{tr}(\rho_1\rho_2)}{\max\left[\mathrm{tr}(\rho_1^2),\mathrm{tr}(\rho_2^2)\right]}. \tag{3.6}$$

This quantity is a fidelity in the sense that it satisfies certain mathematical properties known as Josza axioms [84]. In particular $F_{\max}$ is unity for $\rho_1 = \rho_2$, and is zero for two orthogonal pure states.

3.2.2 Measuring quantum state fidelities

For qubit systems, protocols for measuring theory-experiment fidelities have been recently developed [85, 13, 5, 6]. The idea is that one can represent the theory state ρ_2 as a sum of Pauli strings $\rho_2 = \sum_n c_n\sigma_n$. The task then consists in mesuring in the experimental platforms the terms $\mathrm{tr}(\rho_1\sigma_n)$ for the most representative Pauli strings σ_n based on importance sampling. In our work [65], we adopt a different strategy that allows us to propose the first protocol to measure experiment-experiment fidelities.

The idea behind our protocol is depicted in Fig. 3.3. Each quantum system ρ_1, ρ_2 is subject to randomized measurements $P_u^{(i)}(s) = \langle s|\, u\rho_i u^\dagger\, |s\rangle$, $i = 1, 2$, implemented with the *same* random unitaries u. From this data, we can access the overlap

$$\mathrm{tr}(\rho_1\rho_2) = d^N \sum_{s,s'} (-d)^{-D[s,s']} \overline{P_u^{(1)}(s) P_u^{(2)}(s')}, \tag{3.7}$$

the graphical proof being identical to the one of the purity formula Eq. (2.10):

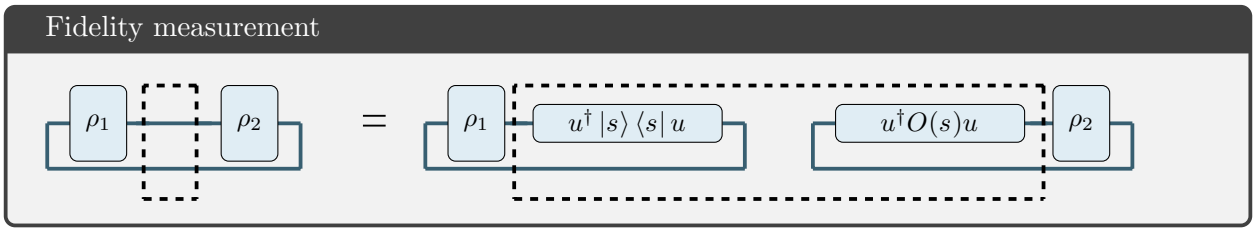

We provide in Ref. [63] a Python code to reconstruct state fidelities for qubit systems. From the overlap, and the purity measurements $\mathrm{tr}(\rho_1^2)$ and $\mathrm{tr}(\rho_2^2)$, obtained using the same experimental data and Eq. (2.10), we obtain the fidelity $F_{\max}$.

3.2.3 Measuring Loschmidt echos

This protocol can be also useful to compare two states $\rho(t)$, and $\rho(t')$ that are prepared in the same experiment, with different evolution times t, t'. The overlap $\mathrm{tr}(\rho(t)\rho(t'))$ is the 'Loschmidt echo', which is an important quantity to describe dynamical quantum phase transitions [86]. In this protocol, randomized measurements are performed on the two quantum states using the same unitaries, and the Loschmidt echo is extracted from the statistical correlations between randomized measurements (here, $\rho_1 \to \rho(t)$, $\rho_2 \to \rho(t')$).

3.2.4 Experimental demonstration

Our protocol could be experimentally demonstrated for the case of theory-experiment fidelities [65]. The experimental state corresponds to the state studied in the case of the Rényi entropies measurements [43]. The data published in this earlier paper provides us with the randomized measurements $P_u^{(1)}(s)$. The second state ρ_2 is obtained from a numerical simulation of the system, including the various sources of decoherence that were measured independently. From this density matrix, we can numerically sample randomized measurements $P_u^{(2)}(s)$.

The measured fidelity is shown in Fig. 3.3, as a function of the size N_A of the subsystem. We observed that the theory state is indeed a faithful representation of the experimental state (~ 0.6 fidelity in the worst case).

One may however wonder why the fidelity is not exactly unity, since we included in the numerical simulations the effect of decoherence. The mismatch is actually due to two effects. First, miscalibration of the random unitaries affect here the measurement by artificially reducing the statistical correlations between measurements. Second, decoherence occuring *during the measurement process*, as described in chapter 1, is also present. These two effects, which were analyzed in details in our work, are not fundamental, as they can be significantly reduced by improving the single-site control of the experiment (in constant progress in various platforms, such as Rydbergs atoms, trapped ions, superconducting qubits,....).

3.3 Many-body topological invariants with randomized measurements

In our work [50], we showed that randomized measurements provide us with a protocol to measure many-body topological invariants of symmetry-protected-topological phases. We also extended this result to the case of two-dimensional topological phases [51].

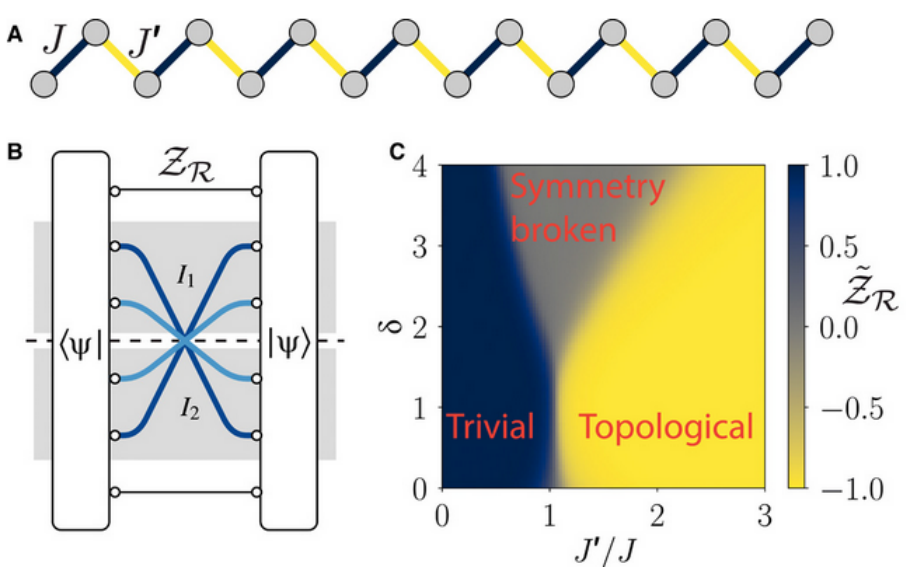

Figure 3.4: (a) Schematic of the extended SSH model. (b) SPT many-body topological invariants $\tilde{Z}_R$ describing the action of reflection symmetry. (c) The MBTI $\tilde{Z}_R$ taking three different quantized values $-1, 0, 1$ can be used to obtain the phase diagram of the SSH model [50].

3.3.1 Introducing symmetry-protected-topological phases and many-body topological invariants

Let us consider for concreteness the extended Su-Schrieffer-Heeger (SSH) model [87, 88, 89]

$$H_{\text{eSSH}} = \frac{J}{2}\sum_{i=1}^{L/2}\left(\sigma^x_{2i-1}\sigma^x_{2i} + \sigma^y_{2i-1}\sigma^y_{2i} + \delta\sigma^z_{2i-1}\sigma^z_{2i}\right) + \frac{J'}{2}\sum_{i=1}^{L/2-1}\left(\sigma^x_{2i}\sigma^x_{2i+1} + \sigma^y_{2i}\sigma^y_{2i+1} + \delta\sigma^z_{2i}\sigma^z_{2i+1}\right). \tag{3.8}$$

This model with $\delta = 0$ was recently implemented with Rydberg atoms [90], and and can also emerge in ultracold atom systems [91, 92].

This model hosts a topological phase, known as the Haldane phase [93] (see Ref. [90] for the mapping to the original spin one formulation), which can be considered as the simplest example of topological phase in a many-body system. Here, topology means that the system in its groundstate cannot be identified from a 'local order parameter', which is a physical quantity associated with a local observable. This differs from the usual scenario of spontaneous symmetry breaking that describes the formation of non-topological phases [94]. The Haldane phase is a symmetry-protected topological phase (SPT), whose origin is due to the presence of *global symmetries* that are encoded in the wavefunction. In the SSH model, we have three symmetries that 'protect' the Haldane phase: (i) spatial reflection symmetry with respect to the center site, (ii) time-reversal symmetry, and (iii) internal symmetries, which are spin rotations of an angle π along the axes x, y and z axes.

Bosonic one-dimensional SPT phases, such as the Haldane phase, can be formally classified based on the theory of group cohomology, which can describe the formal representation of symmetries in a many-body wavefunction [95, 96]. Recently, remarkable theory works have shown that one can extract such symmetry representations based on many-body topological invariants (MBTIs) [97, 98]. The MBTIs are functions of the reduced density matrix ρ of size L in a lattice system, and take a quantized value $0, \pm 1$ in the thermodynamics limit $L \gg \ell_c$ (ℓ_c is the correlation

length of the system). This raised an obvious interest for developing protocols that could measure these MBTIs, with the prospect to be able to classify SPT phases in an experiment.

3.3.2 Randomized measurement protocols

MBTI are highly non-local and non-linear functionals of the density matrix. In our work [50], we relate MBTI to statistical correlations of randomized measurements. The key difference compared to our previous protocols is that we use distributions of random unitaries that can incorporate the symmetries of the system.

Partial-reflection invariant

The partial reflection invariant was introduced to extract the symmetry representation of a wave-function with respect to spatial reflection symmetry [98]. We consider a subsystem of $2L$ sites, and the reflection operator $\mathcal{R}$ that transforms the basis states $|s\rangle = |s_1, \ldots, s_{2L}\rangle$ into their mirrored images $\mathcal{R}|s\rangle = |s_{2L}, \ldots, s_1\rangle$. Pollmann and Turner have shown that the quantity $\mathcal{Z}_\mathcal{R} = \mathrm{tr}(\rho\mathcal{R})$ can be used to define a MBTI [98]. Indeed, if one denotes as I_1 the first $\{1, \ldots, L\}$ sites, and by $I_2 = \{2L, \ldots, L+1\}$ the rest of the subsystem, the quantity

$$\tilde{\mathcal{Z}}_\mathcal{R} \quad = \quad \frac{\mathcal{Z}_\mathcal{R}}{\sqrt{\mathrm{tr}(\rho_{I_1}^2)}} \tag{3.9}$$

is quantized in the thermodynamic limit $L \to \infty$, and extract the symmetry representation of partial-reflection symmetry [98]. The structure of $\mathcal{Z}_\mathcal{R}$ is illustrated in Fig. 3.4b), while the phase diagram showing the quantized values of the MBTI $\tilde{\mathcal{Z}}_\mathcal{R}$ in the extended SSH-model is represented in Fig. 3.4c).

The structure of MBTIs can be understood graphically. Here, the quantity $\mathcal{Z}_\mathcal{R}$ can be seen as a highly non-local quantity that results from the contraction of the indices s_{I_1} of the subsystem I_1 with the ones s_{I_2} of I_2, c.f., below.

After a few steps of randomized measurements surgery, shown in this graphics, we can rewrite $\mathcal{Z}_\mathcal{R}$ in terms of statistical correlations of randomized measurements.

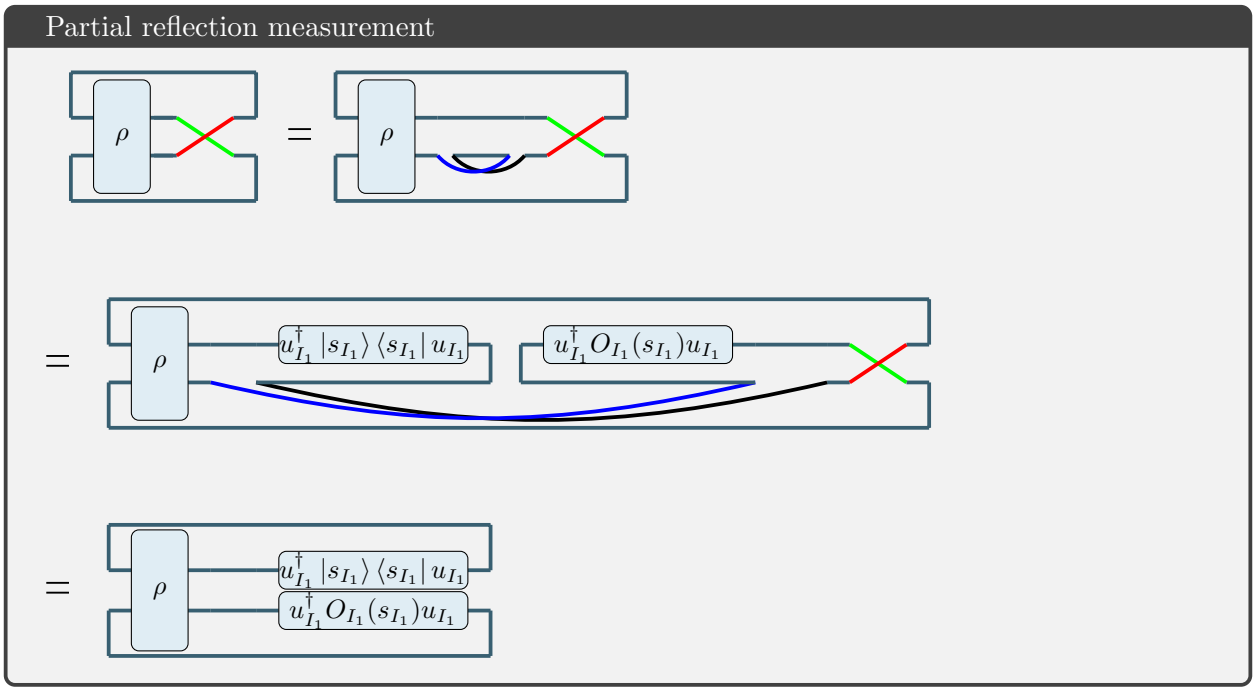

Inserting, as in the previous section, the value of the operator $O(s_{I_1})$, and averaging over all 2^L basis states s_{I_1}, we obtain

$$\mathcal{Z}_{\mathcal{R}} = 2^L \sum_s (-2)^{-D[s_{I_1}, s_{I_2}]} \overline{P_u(s)}, \tag{3.10}$$

with the random unitary $u = u_{I_1} \otimes u_{I_1}$, $u_{I_1} = u_1 \otimes \cdots \otimes u_L$, and $u_{i=1,\ldots,L}$ is sampled independently from a local 2−design, is a reflection symmetric random unitary. This results provides a measurement protocol for $\mathcal{Z}_{\mathcal{R}}$ and therefore for $\tilde{\mathcal{Z}}_{\mathcal{R}}$. At a conceptual level, Eq. (3.10) shows that we can interpret the MBTI as the quantized response of a system to a reflection-symmetric random perturbation.

Time-reversal invariant

The MBTI associated with time-reversal symmetry was introduced in Refs. [98, 99, 100]. In order to define the MBTI, the subsystem ρ is again divided into two parts I_1 and I_2, whose states are here indexed as $s_{I_1} = s_1, \ldots, s_L$, and $s_{I_2} = s_{L+1}, \ldots, s_{2L}$. The MBTI associated with time-reversal symmetry can be written as

$$\begin{aligned} \tilde{\mathcal{Z}}_{\mathcal{T}} &= \frac{\mathcal{Z}_{\mathcal{T}}}{\left[\mathrm{tr}(\rho_{I_1}^2)\right]^{3/2}} \\ \mathcal{Z}_{\mathcal{T}} &= \mathrm{tr}(u_{\mathcal{T}}^\dagger \rho u_{\mathcal{T}} \rho^{T_{I_1}}), \end{aligned} \tag{3.11}$$

with $u_{\mathcal{T}}$ the unitary matrix representing the 'unitary part' of the time-reversal operation, and $\rho^{T_{I_1}}$ the partially transposed density matrix, which is defined via

$$\langle s_{I_1}, s_{I_2}| \rho^{T_{I_1}} |s'_{I_1}, s'_{I_2}\rangle = \langle s'_{I_1}, s_{I_2}| \rho |s_{I_1}, s'_{I_2}\rangle . \tag{3.12}$$

Once again, the stucture of the MBTI can be better understood graphically, and then manipulated to be re-expressed in terms of randomized measurements.

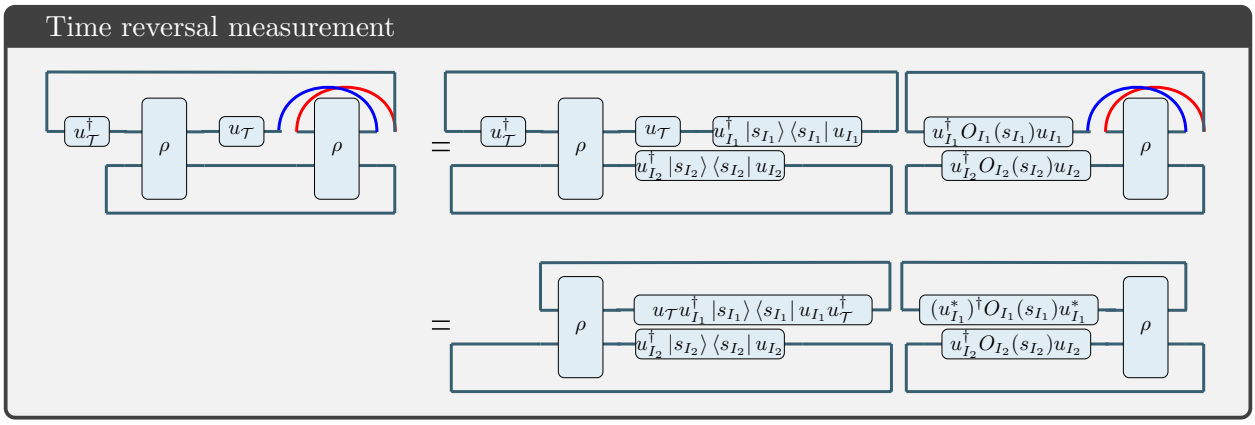

To write the second equality, we have used the property

$$(v^\dagger o v)^T = v^T o^T (v^\dagger)^T = (v^*)^\dagger o v^*, \tag{3.13}$$

with the unitary $v = u_{I_1}$ and the diagonal operator $o = O_{I_1}(s_{I_1})$. Averaging over all 2^{2L} states $s = (s_{I_1}, s_{I_2})$, we obtain

$$\mathcal{Z}_{\mathcal{T}} = 2^{2L} \sum_{s,s'} (-2)^{-D[s,s']} \overline{P_u^{(1)}(s) P_u^{(2)}(s')}, \tag{3.14}$$

with $P_u^{(1)}(s) = \langle s| u^{(1)} \rho (u^{(1)})^\dagger |s\rangle$, $u^{(1)} = (u_{I_1} u_{\mathcal{T}}^\dagger) \otimes u_{I_2}$, and $P_u^{(2)}(s) = \langle s| u^{(2)} \rho (u^{(2)})^\dagger |s\rangle$, $u^{(2)} = (u_{I_1})^* \otimes u_{I_2}$. Here, $u_{I_1} = u_1 \otimes \cdots \otimes u_L$, and $u_{I_2} = u_{L+1} \otimes \cdots \otimes u_{2L}$ are two independent random unitaries.

Internal symmetries invariant

The D_2 invariant measuring internal spin symmetries was the first MBTI introduced for SPT phases [97, 98]. Here, we consider a subsystem that is made of three consecutive regions I_1, I_2 and I_3, each of them having L sites. The MBTI $\tilde{\mathcal{Z}}_{D_2}$ is defined as

$$\begin{aligned} \tilde{\mathcal{Z}}_{D_2} &= \frac{\mathcal{Z}_{D_2}}{\mathrm{tr}(\rho_{I_1}^2)^2} \\ \mathcal{Z}_{D_2} &= \mathrm{tr}\left(S_{I_1} (P_{I_2} \otimes P_{I_2}) S_{I_3} (V_{I_1} \rho V_{I_1}^\dagger \otimes \rho) \right). \end{aligned} \tag{3.15}$$

Here, S_{I_i} is the swap operator $S_{I_i} |s_{I_i}\rangle \otimes |s'_{I_i}\rangle = |s'_{I_i}\rangle \otimes |s_{I_i}\rangle$, P_{I_2} is a diagonal operator in the computational basis, namely $P_{I_2} = \sum P_{I_2}(s_{I_2}) |s_{I_2}\rangle\langle s_{I_2}| = \prod_{i \in I_2} \sigma_i^z$, and $V_{I_1} = \prod_{i \in I_1} \sigma_i^x$. Once again, the structure of the MBTI is better understandable graphically, which allows us at the same time to derive a randomized measurement protocol:

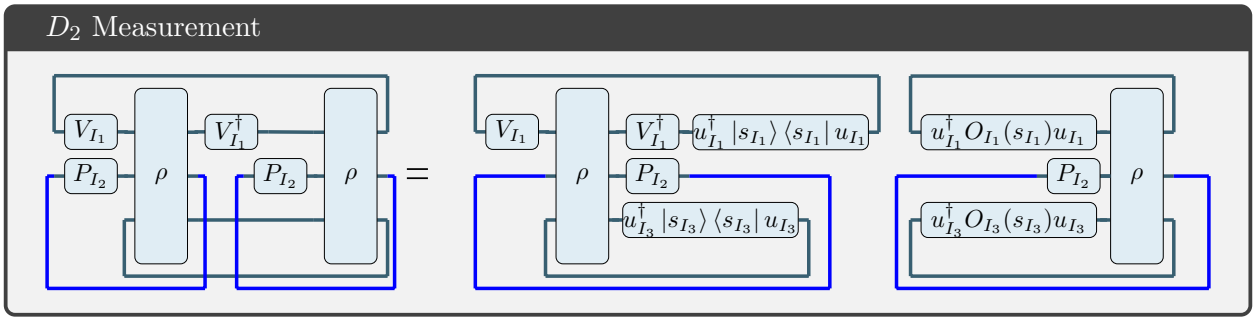

The final result of this derivation (averaging over all 2^{2L} states s_{I_1} and s_{I_3}) is

$$\mathcal{Z}_{D_2} = 2^{2L} \sum_{s,s'} (-2)^{-D[s_{I_1\cup I_3}, s'_{I_1\cup I_3}]} P_{I_2}(s_{I_2}) P_{I_2}(s'_{I_2}) \overline{P_u^{(1)}(s) P_u^{(2)}(s')}, \tag{3.16}$$

with the two randomized measurements $P_u^{(1)}(s) = \langle s| u^{(1)} \rho (u^{(1)})^\dagger |s\rangle$, $u^{(1)} = u_{I_1} V_{I_1} \otimes 1_{I_2} \otimes u_{I_3}$, and $P_u^{(2)}(s) = \langle s| u^{(1)} \rho (u^{(1)})^\dagger |s\rangle$, $u^{(2)} = u_{I_1} \otimes 1_{I_2} \otimes u_{I_3}$.

3.4 Randomized measurement of the many-body Chern number

Building on the remarkable theory and experimental efforts on probing integer quantum Hall states (see e.g. the review [101]), we have recently extended our approach for measuring topological invariants of fractional quantum Hall states [51]. The many-body Chern number (MBCN), which is the many-body topological invariant relevant for lattice versions of fractional quantum Hall states, can be written in a form that is suitable for randomized measurements. In contrast to previous approaches based on linear response perturbations [102, 103, 104, 105], our protocol extracts the MBCN from measurements on the wavefunction, without relying on auxiliary systems.

Consider for concreteness the groundstate $|\psi\rangle$ of a hard-core boson model implemented on the square lattice geometry shown in Fig. 3.5. We define a subsystem made of two parts R_1, and R_2, of size $\ell_1 \times \ell_y$, and $\ell_2 \times \ell_y$, respectively. The many-body Chern number can be written as a function of the reduced state ρ as [51, 106]

$$\begin{aligned} C &= \arg(\mathcal{T}(\theta_x)) \\ \mathcal{T}(\theta_x) &= \mathrm{tr}\left(S_{R_1} \left[P_{R_2}(\theta_x) \otimes P_{R_2}(\theta_x) \right] \left[V_{R_1} \rho V_{R_1}^\dagger \otimes \rho \right] \right), \end{aligned} \tag{3.17}$$

with $V_{R_1} = \prod_{(x,y)\in R_1} \exp(i2\pi \tilde{s}(y/\ell_y) n(x,y))$, and $P_{R_2}(\theta_x) = \prod_{(x,y)\in R_2} \exp(i\theta_x n(x,y))$ ($n(x,y)$ is the boson density). Here $\tilde{s}$ is an integer that controls the number of 'flux quantas' injected via V_{R_1}. The derivation of Eqs (3.17) is based on topological quantum-field theory, and consists in rewriting the partition function of the groundstate on topological space-time geometries [51, 106]. Having in mind a measurement protocol, this formulation of the MBCN is simpler compared to the original one that is given on torus geometries with twisted boundary conditions [107].

It is interesting to note that the function $\mathcal{T}(\theta_x)$ has the same form as the MBTI $\mathcal{Z}_{D_2}$[1]. This implies that, in direct analogy with the measurement of $\mathcal{Z}_{D_2}$, we can measure $\mathcal{T}(\theta_x)$ via randomized measurements. The corresponding experimental protocol is depicted in Fig. 3.5. The numerical simulations of statistical errors (right panel) demonstrate that the MBCN can be faithfully estimated in experimental setups with fast repetition rates (superconducting qubits, Rydberg atoms, trapped ions, ...).

[1] Note that the same connection was first observed in Ref. [108] for a different form of the MBTIs.

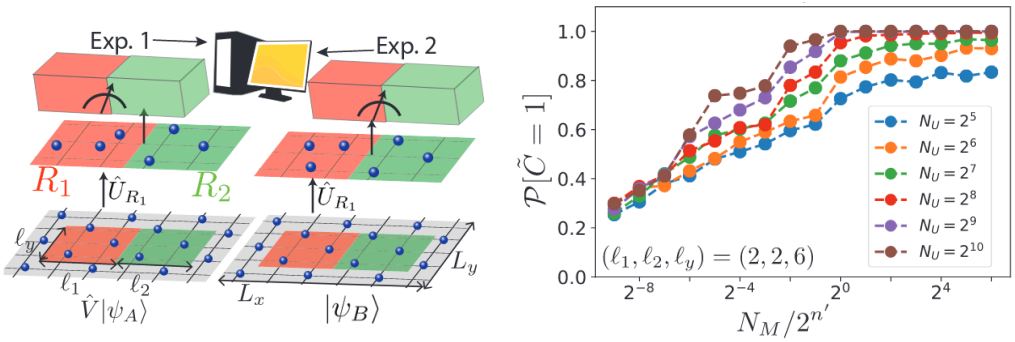

Figure 3.5: Randomized measurement of the many-body Chern number in a two-dimensional square lattice [51]. In the right panel, the probability to identify the system in the topological phase is represented as a function of the number of randomized measurements.

Chapter 4

High-order functionals of the quantum state from randomized measurements

As shown in the two previous chapters, we have developed a powerful toolbox for estimating entanglement entropies, out-of-time-order correlators, many-body topological invariants, etc, which are quantities associated with *second-order polynomials* of density matrices or operators, e.g., the purity $\mathrm{tr}(\rho^2)$. In the following, we present our work [14], showing how to extend the randomized measurement toolbox to access higher-order polynomials of ρ, and how to apply these new ideas for probing mixed-state entanglement of many-body systems.

4.1 Motivation: the positive-partial transpose condition

The entanglement condition based on Eq. (1.9) is useful to detect bipartite entanglement for a nearly-pure state $\mathrm{tr}(\rho_{AB}^2)$, such as in the 10-qubit system in Ref. [43]. For generic mixed states, this condition typically fails in detecting entanglement, and one has to consider more advanced tests [18]. This situation is particularly relevant for experiments in the regime of quantum advantage, where only (mixed) subsystems can be measured.

Here, we consider the positive-partial transpose criterion (PPT) [109] (see also Refs. [18, 24] for reviews, including relations to other conditions). Consider a separable state, then the partially tranposed (PT) density matrix $\rho_{AB}^{T_A}$ (as defined in Eq. (3.12)) can be written as

$$\rho_{AB}^{T_A} = \sum_k c_k \left[(\rho_A^{(k)})^T \otimes \rho_B^{(k)} \right], \tag{4.1}$$

with $0 \leq c_k \leq 1$. As $\rho_A^{(k)}$ and $\rho_B^{(k)}$ are positive semi-definite matrices, the matrices $(\rho_A^{(k)})^T \otimes \rho_B^{(k)}$ are positive semi-definite, and therefore $\rho_{AB}^{T_A}$ is also positive semi-definite. *Thus, the PPT criterion states that, for any separable state, the matrix $\rho_{AB}^{T_A}$ does not have any negative eigenvalues.* Remarkably, the PPT criterion has been shown to be, not only a necessary, but also a sufficient condition for diagnosing the separability of two qubits (or two qutrits), i.e., all entangled states have in this case at least one negative eigenvalue [110]. For higher dimensional systems, the PPT criterion, as necessary condition of separability, can be used to detect entanglement.

The entanglement monotone associated with the PPT criterion is the negativity [111]

$$\mathcal{N}(\rho_{AB}) = \sum_{\lambda<0} |\lambda|, \tag{4.2}$$

with $\{\lambda\}$ the spectrum of $\rho_{AB}^{T_A}$. The negativity can obviously be used to detect entanglement: If $\mathcal{N}(\rho_{AB}) > 0$, $\rho_{AB}^{T_A}$ is not positive semi-definite, and therefore the state is entangled. The negativity, as entanglement monotone, has been also studied to quantify entanglement in many-body states in condensed matter [112, 113, 114, 115, 116, 117, 118, 119, 120, 121, 122].

Instead of the negativity, we are interested in measuring simpler quantities, which are built from polynomials of the partially transpose density matrix

$$p_n = \mathrm{tr}\left[\left(\rho_{AB}^{T_A}\right)^n\right], \tag{4.3}$$

with $n = 1, 2, \ldots$. In the context of quantum field theories, these quantities, which we here call PT moments, have been shown to have the same universal properties as the negativity [114, 123, 124, 125].

4.2 Mixed-state entanglement from local randomized measurement

First, it is worth noting that the third PT is the first moment that carries information about the partial transpose operation. Indeed, as shown graphically below, $p_1 = 1$, and $p_2 = \mathrm{tr}(\rho_{AB}^2)$ is the purity of the original state ρ_{AB}.

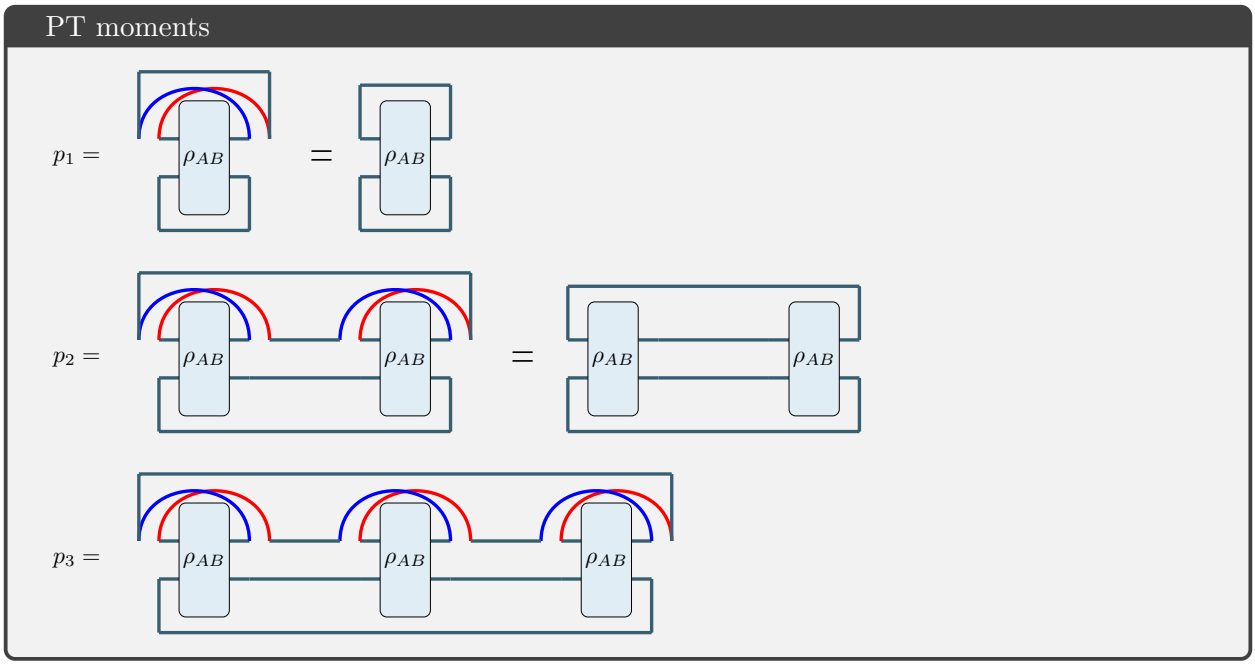

In the following, we first present our randomized measurement protocol for PT moments. We then show that p_3 can be used to define a powerful entanglement condition that is connected to the PPT criterion.

4.3 PT moments from local randomized measurements

Theory protocols have already been proposed to measure p_3 and higher order moments using physical copies [126] and global randomized measurements [127]. In Ref. [14], we propose and

demonstrate an experimentally-friendly protocol to measure p_n, $n \geq 3$, with local random unitaries.

4.3.1 Warm-up: Randomized measurement tomography

The first ingredient for our protocol originates from an earlier work [47], where we proved that local randomized measurements are 'tomographically complete'. This means that, assuming that we can perform a sufficient number of projective measurements $N_M \times N_U$, we can reconstruct the full density matrix

$$\rho_{AB} \quad = \quad d^N \sum_{s,s'} (-d)^{-D[s,s']} \overline{P_u(s) u^\dagger \left|s'\right\rangle \left\langle s'\right| u}, \tag{4.4}$$

which we here prove graphically (using the same notations as in chapter 2)

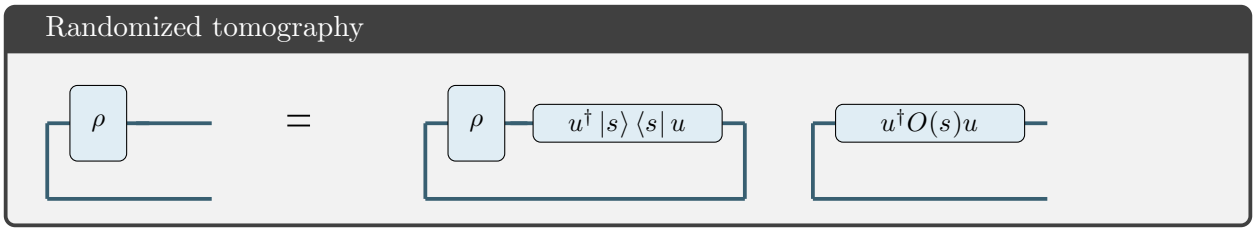

Note that this identity was also proven in the $N = 1$ case in the context of the Hubbard model in Ref. [56].

4.3.2 Protocol

The key idea behind our protocol is that we can use Eq. (4.4), not for doing tomography and reconstructing the state ρ, but to access directly PT moments from randomized measurements. To simplify our notations, let us consider the limit $N_M = 1$, with a single projective measurement $s_r = (s_{r1}, \ldots, s_{rN})$ for each random unitary u_r, $r = 1, \ldots, N_u$. In this case, Eq. (4.4) can be written as $E[\rho_{AB}^{(r)}] = \rho_{AB}$ with

$$\rho_{AB}^{(r)} \quad = \quad \bigotimes_{i=1}^{N} \left[(d+1) u_r^\dagger \left|s_{ri}\right\rangle \left\langle s_{ri}\right| u_r - \mathbf{I_d} \right], \tag{4.5}$$

with the expectation value E over random unitaries *and* projective measurements. The advantage of this framework is that it provides us with unbiased estimators of polynomial functions of ρ_{AB} based on U-statistics [62]. This simply consists in replacing each term ρ_{AB} appearing in the expression of p_n by a term $\rho_{AB}^{(r)}$. This idea was first presented in Ref. [53] to obtain a new statistical estimator for the purity

$$p_2^{(e)} = \left[\mathrm{tr}(\rho_{AB}^2)\right]^{(e)} = \frac{1}{N_u(N_u-1)} \sum_{r \neq r'} \mathrm{tr}\left[\rho_{AB}^{(r)} \rho_{AB}^{(r')}\right], \tag{4.6}$$

which can lead to reduced statistical errors compared to our estimator Eq. (2.20) (in a particular error regime and at the cost of miscalibration errors [14]). As presented in our work [14], we can simply generalize this method to access p_3 (and, similarly, higher order moments) via

$$p_3^{(e)} = \frac{1}{N_u(N_u-1)(N_u-2)} \sum_{r \neq r' \neq r''} \mathrm{tr}\left[(\rho_{AB}^{(r)})^{T_A} (\rho_{AB}^{(r')})^{T_A} (\rho_{AB}^{(r'')})^{T_A}\right]. \tag{4.7}$$

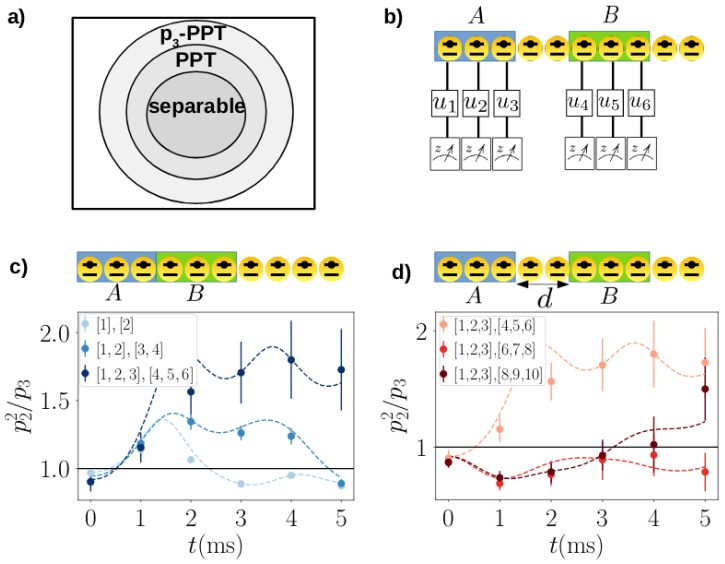

Figure 4.1: PT moments via local randomized measurements [14] a) Relation between the p_3-PPT condition and the PPT condition, (b) Measurement protocol, (c) and (d) Experimental demonstration of mixed state entanglement using the p_3-PPT condition.

How exactly does our protocol differ from what is done in tomography? Here, we extract via Eq. (4.7) the PT moment p_3 from a direct multilinear operation on the measured bitstrings, i.e., we do not build a tomographic representation of ρ (which would be obviously costly in terms of runtime and memory usage). Instead, the postprocessing task consists in simply calculating overlap between tensor-product states $\rho_{AB}^{(r)}$, a procedure that is cheap and scalable. Also, the framework of U-statistics guarantees 'unbiased' estimations, meaning that even for a finite number of measurements, we obtain in average the right value of p_3. Finally, our analytical error study shows that the typical number of measurements to obtain p_2, p_3 with a given accuracy is of the order of 2^N, which is again exponentially smaller than the required number $\sim 4^N$ for tomography [14].

4.3.3 Entanglement detection via the p_3-PPT condition

For the purpose of detecting entanglement via the PPT criterion, PT moments can be used to extract the negativity based on Chebyshev (or machine-learning) interpolation-based methods [126]. In our case, we were interested instead in using directly the value of p_3 for entanglement detection. To do so, we derived the following 'p_3-PPT condition'

$$\rho_{AB} \in \text{PPT} \implies p_3 > p_2^2. \tag{4.8}$$

Conversely, if $p_3 < p_2^2$, then the states violates the PPT condition, and is therefore entangled. This connection is illustrated graphically in Fig. 4.1a).

In order to prove the p_3-PPT condition Eq. (4.10), one first defines

$$X_f = \text{tr}[f(\rho_{AB}^{T_A})] = \sum_\lambda \text{tr}[f(\lambda)], \tag{4.9}$$

with f a polynomial. From this equality, we see that, if our polynomial f satisfies $f(x) \leq 0$ for $x \geq 0$

$$\rho_{AB} \in \text{PPT} \implies \forall \lambda, \lambda \geq 0 \implies X_f \leq 0 \tag{4.10}$$

One possible choice for such f is $f_a(x) = -x(x-a)^2$, a being a real number, and therefore

$$\rho_{AB} \in \text{PPT} \implies X_{f_a} = -p_3 + 2ap_2 - a^2 \leq 0. \tag{4.11}$$

In order to obtain the most powerful condition that can detect the maximum number of entangled states, we can choose the value of a which maximizes the value of X_{f_a}. This maximum is obtained for $a = p_2$, leading to $X_{f_a} = -p_3 + p_2^2$, and therefore to the p_3-PPT condition Eq. (4.10).

4.3.4 Experimental demonstration

We have tested the ability of the p_3-PPT condition to detect entanglement on various states, including Werner states where this condition is shown to be equivalent to the PPT condition. Furthermore, we have analyzed the experimental data of Ref. [43] to provide the first measurement of p_3. Based on this measurement, we could demonstrate mixed-state entanglement via the p_3 condition, see Fig. 4.1c), d), and also study the propagation of entanglement based on the normalized ratio $p_3/\text{tr}(\rho_{AB}^3)$ [114].

Chapter 5

Outlook

Building on the seminal work of van Enk and Beenakker [44], we have shown that randomized measurements can be implemented in various platforms, and used to measure many physical quantities related to quantum entanglement. These results act as a motivation to continue developing the randomized measurement toolbox. I describe below four research directions that I would like to investigate.

5.1 Optimization of randomized measurements protocols

The measurement budget, i.e., the question of the required number of measurements to obtain a faithful estimation, is a crucial aspect for a measurement protocol. For randomized measurement protocols, we have identified an exponential scaling of the measurements $\sim 2^{\alpha n}$ (with here n qubits), with relatively small exponent $\alpha \sim 1$. This type of 'friendly' exponential scaling has allowed us to measure entanglement entropies, fidelities, etc for the largest system sizes so far, of sizes $n = 10$ [43]. Preskill et al have now established that such scaling should indeed be generically expected when measuring quantities such as the purity [53]. This implies that our statistical estimators are probably optimal (in terms of scaling) in the situation that we considered so far, where all the measurement data is acquired *before* an estimation is made.

To improve randomized measurement protocols, we would like to develop a strategy based on analyzing measurement data *iteratively*, and using the tools of Monte Carlo integration. Our idea consists in running an importance sampling algorithm such as 'MISER' [128] on a classical computer that is coupled to the quantum device subject to randomized measurements. (i) First, the algorithm randomly chooses a few random unitaries, which are sent to the quantum device. (ii) The corresponding randomized measurements are then analysed by MISER, which based on statistical error analysis identifies the measurements to be performed in the quantum unit in the next iteration. Step (ii) is finally repeated until desired accuracy is reached. In the end, the random unitaries will be chosen adaptively, with significant reduction of the measurement budget.

5.2 Multipartite entanglement

We would like to study whether statistical correlations between randomized measurements contain information beyond bipartite entanglement. For this, we would like to show that the quantum information quantities that relate to multipartite entanglement, i.e., entanglement between three, four, etc , parts of a system, can be 'extracted'. This can be done based on two approaches.

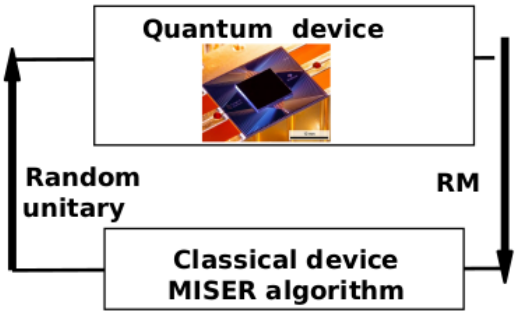

Figure 5.1: Optimization of randomized measurements via a classical-quantum hybrid algorithm.

5.2.1 Protocol to measure the quantum Fisher information

The quantum Fisher information (QFI) has emerged as a fundamental quantity to characterize multipartite entanglement. Above a certain value ($F_Q \geq kN$, N number of spins), the QFI certifies that at least k particles are genuinely entangled, i.e., it is not possible to write the quantum state as a mixture of density matrices that are factorized in terms involving less than k particles [129]. The QFI is also fundamental for quantum metrology, as it defines the set of entangled states that provide an advantage over classical states for parameter estimations. Due to its nontrivial relation to the density matrix, the QFI has never been measured for a large generic many-body state.

We believe that randomized measurements protocols provide an answer to this measurement challenge. First, we would like to provide a protocol to measure the quantum asymmetry [130]

$$\mathcal{A} = 4\frac{\mathrm{tr}(\rho^2) - \mathrm{tr}(\rho e^{-i\theta H}\rho e^{i\theta H})}{\theta^2}, \tag{5.1}$$

which is a lower bound to the QFI. The asymmetry has an expression that is reminiscent of a 'state fidelity' which we know how to measure, see chapter 3. However, the role of statistical errors, and therefore experimental feasibility, will be very different as asymmetry measures a 'relative' state overlap with respect to an unknown quantum state.

Having via the measurement of asymmetry a *lower* bound of the QFI means that we can certify that some states are multipartite entangled, while the test can remain unconclusive for some other entangled states. We will therefore also derive a protocol to access the quantum Fisher information. Here, the idea is that we can express the QFI as a polynomial decomposition of ρ, which can be estimated 'efficiently' using randomized measurements (chapter 4).

5.2.2 Multipartite entanglement from a set a bipartite entanglement measures

In Ref. [43], we could measure the Rényi entropies of all 1024 bipartitions of a 10-ion quantum simulators. A natural question is whether, by combining all these numbers, one can make a precise statement about multipartite entanglement. Several theoretical attempts have been made to answer this question in the few qubit case [131, 132]. In particular, 'sector lengths' quantifying the amount of k-particles correlations can be extracted from second Rényi entropies.

We would like to understand which other characteristics of multipartite entanglement can be extracted from combinations of bipartite entanglement quantifiers: e.g. entanglement depth [131], or other recent and promising measures such as the joint-Schmidt decomposition that provides a decomposition of quantum states for many partitions of the system simultaneously [133].

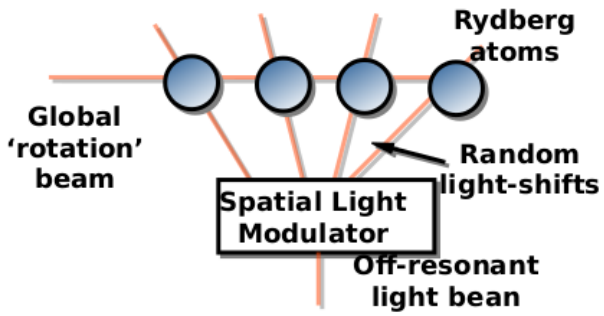

Figure 5.2: Implementation of local random unitaries with Rydberg atoms

5.3 A measurement toolbox for cold atoms

Randomized measurement protocols can be routineley used to probe entanglement in trapped ions experiments [43, 14, 49], superconducting qubits [134], NMR systems [82], because these platforms benefit from local addressing techniques, i.e., each qubit can be controlled individually.

We would like to develop ideas to physically implement randomized measurements with Rydberg atoms, and ultracold atoms, which suffer from constraints regarding local addressing.

5.3.1 Rydberg atoms

Rydberg atoms represent a promising platform for quantum technologies, with clear potential for scalability and implementations of spin models for quantum simulation [90]. However, the Rydberg atoms encoding the spins cannot be yet fully addressed locally, i.e., it is usually not possible to apply a specific local rotation on each spin individually.

Even if we do not know how to realize *a specific* local unitary operation on each spin, we can still produce *an ensemble* of local random unitaries described in good approximation by a certain random ensemble. A possible approach is depicted in Fig. 5.2. One could think of using a spatial light modulator to imprint on each atom a random energy shift, which is combined with a laser beam that can globally flip the state of the atom. These light beams will make each atomic spin randomly precess on their Bloch sphere. After some finite time evolution, the rotations applied on each spin will become statistically independent, each of them described in good approximation by the circular unitary ensemble (CUE) of random matrix theory. This is the only required ingredient to implement randomized measurements.

Once a recipe for random spin rotations has been proposed and implemented, a series of experiments in collaboration with the Browaeys group [90] has been planned, such as the measurement of many-body topological invariants [50].

5.3.2 Protocols for Hubbard models

For Hubbard models, as realized with ultracold atoms, the total number of particles is conserved and thus elementary random operations cannot be purely local (the elementary process, atom tunneling, involves two sites). There is however a growing interest for applying randomized measurements in these systems. This is motivated by the facts that (i) atoms offer large coherence time compared the typical interaction time scales, (ii) entanglement can reveal unique features of atomic Hubbard models [135, 136], (iii) ultracold atom setups are equipped with quantum gas microscopes [137], or

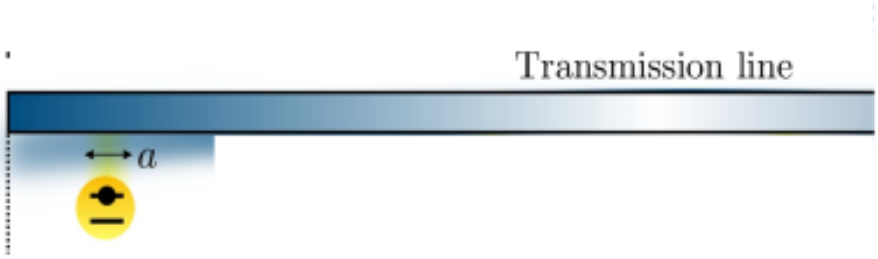

Figure 5.3: Schematic of the system implemented in N. Roch's experiment at Institut Néel (Grenoble).

high-resolution time-of-flight imaging [138], which can projectively measure particles at the single-atom level.

In order to develop a randomized measurements protocol for measuring entanglement in Hubbard models, the challenge is to find strategies to generate random unitary matrices, which are reproducible, and whose statistical properties can be described with a random matrix theory that incorporates conservation laws. While we have presented a first method in Ref. [45], based on the original van Enk's protocols [44], we would like to propose an experimentally friendly new approach, which is inspired by our protocols for spin systems [45, 43].

Instead of using spin rotations, we will consider non-interacting random unitaries in Hubbard models as basic building blocks for these protocols. To show that this is sufficient to access quantities like entanglement entropies, we will extend the random matrix theory framework that we have developed for local spin rotations to such random operations.

5.4 Entanglement in quantum impurity models

With N. Roch and S. Florens (Néel Institute), and Anna Minguzzi (LPMMC), we have started a collaboration to study and detect entanglement in Josephson junctions circuits. Nicolas Roch and colleagues have shown that a superconducting quantum device, made of strong nonlinear Josephson Junction coupled to a waveguide (fig. 5.3) is a promising quantum simulation platform for quantum impurity models, such as the Kondo model [139].

Our goal will be to understand the role of entanglement in this system. For this, we will perform large-scale numerical simulations of the system with Density-Renormalization-Group (DMRG) techniques, and extract entanglement entropies.

Then, we will investigate whether one can experimentally measure such entanglement entropies. The situation significantly differs from the standard scenario of randomized measurements, as the impurity can only be probed by measuring the photons that leave the waveguide. A possible strategy is to consider random changes of the parameters of the junction, and to relate, via random matrix theory, the statistical distribution of measurements performed on the output field to the density matrix of the impurity.

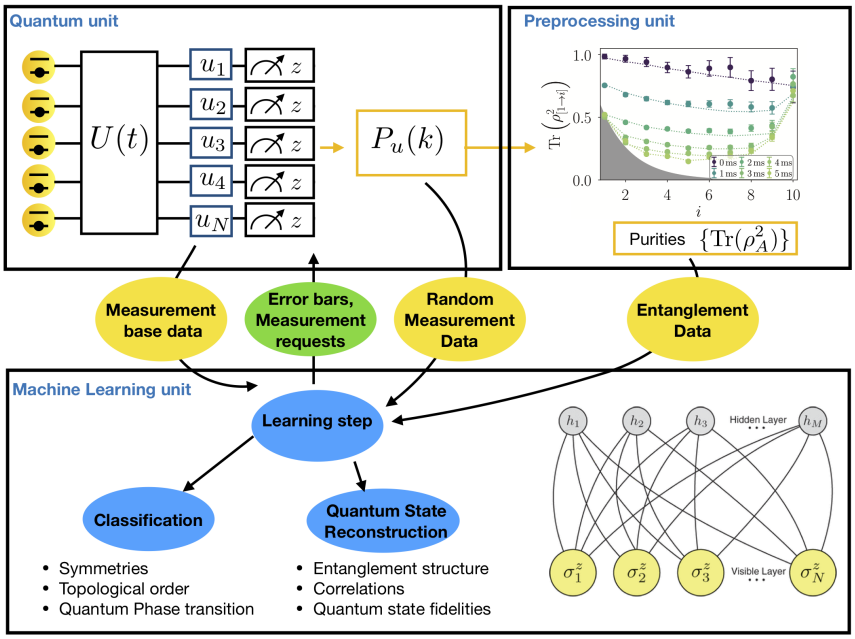

Figure 5.4: *Machine learning of quantum states* Our approach will consist in feeding a machine learning algorithm with data obtained from randomized measurements, and in obtaining as output a classification of the different features of the quantum states, and a quantum state reconstruction in terms of a neural network.

5.5 Mid-term goal: Machine-learning assisted data processing of quantum experiments

In the future, we would like to combine our approaches with machine learning algorithms for classification, and quantum state reconstruction [140, 141, 7, 8, 142, 143, 144]. These methods consist in extracting features of a quantum state using the tools of data science, and using as input datasets of measurements, for example spin populations in a single basis [7]. This is achieved by training and sampling neural networks representing the quantum state, where entanglement or correlations are encoded in different layers of neurons.

One possibility would be to design and use a machine learning algorithm with a large set of data obtained from a "quantum unit". The key advantage of this approach is that we could construct neural networks without a preferential measurement basis. This technique would allow thus to extract key information, such as entanglement and topological order, without any assumption on the quantum state.

A schematic is shown in Fig. 5.4. This data acquired from the quantum unit will be sent to the classical machine learning unit, together with the information about random unitaries, and "preprocessed" data obtained by analyzing statistical correlations, in order for instance to estimate the purity of the quantum state. This preprocessed data could be used for example to adapt the type of neural network and numerical approach to be used for the training stage. The machine learning algorithm could be then used to classify quantum states, or to provide a reconstruction of a quantum state based on the neural network ansatz.

Bibliography

[1] I. M. Georgescu, S. Ashhab, and F. Nori, Reviews of Modern Physics **86**, 153 (2014).

[2] J. Preskill, Quantum **2**, 79 (2018).

[3] D. Gross, Y. K. Liu, S. T. Flammia, S. Becker, and J. Eisert, Physical Review Letters **105**, 150401 (2010).

[4] C. Song, K. Xu, W. Liu, C.-p. Yang, S.-B. Zheng, H. Deng, Q. Xie, K. Huang, Q. Guo, L. Zhang, P. Zhang, D. Xu, D. Zheng, X. Zhu, H. Wang, Y.-A. Chen, C.-Y. Lu, S. Han, and J.-W. Pan, Physical Review Letters **119**, 180511 (2017).

[5] M. Cramer, M. B. Plenio, S. T. Flammia, R. Somma, D. Gross, S. D. Bartlett, O. Landon-Cardinal, D. Poulin, and Y.-K. Liu, Nature Communications **1**, 149 (2010).

[6] B. P. Lanyon, C. Maier, M. Holzäpfel, T. Baumgratz, C. Hempel, P. Jurcevic, I. Dhand, A. S. Buyskikh, A. J. Daley, M. Cramer, M. B. Plenio, R. Blatt, and C. F. Roos, Nature Physics **13**, 1158 (2017).

[7] G. Torlai, G. Mazzola, J. Carrasquilla, M. Troyer, R. Melko, and G. Carleo, Nature Physics **14**, 447 (2018).

[8] G. Torlai and R. G. Melko, Physical Review Letters **120**, 240503 (2018).

[9] F. Arute, K. Arya, R. Babbush, D. Bacon, J. C. Bardin, R. Barends, R. Biswas, S. Boixo, F. G. S. L. Brandao, D. A. Buell, B. Burkett, Y. Chen, Z. Chen, B. Chiaro, R. Collins, W. Courtney, A. Dunsworth, E. Farhi, B. Foxen, A. Fowler, C. Gidney, M. Giustina, R. Graff, K. Guerin, S. Habegger, M. P. Harrigan, M. J. Hartmann, A. Ho, M. Hoffmann, T. Huang, T. S. Humble, S. V. Isakov, E. Jeffrey, Z. Jiang, D. Kafri, K. Kechedzhi, J. Kelly, P. V. Klimov, S. Knysh, A. Korotkov, F. Kostritsa, D. Landhuis, M. Lindmark, E. Lucero, D. Lyakh, S. Mandrà, J. R. McClean, M. McEwen, A. Megrant, X. Mi, K. Michielsen, M. Mohseni, J. Mutus, O. Naaman, M. Neeley, C. Neill, M. Y. Niu, E. Ostby, A. Petukhov, J. C. Platt, C. Quintana, E. G. Rieffel, P. Roushan, N. C. Rubin, D. Sank, K. J. Satzinger, V. Smelyanskiy, K. J. Sung, M. D. Trevithick, A. Vainsencher, B. Villalonga, T. White, Z. J. Yao, P. Yeh, A. Zalcman, H. Neven, and J. M. Martinis, Nature **574**, 505 (2019).

[10] J. Emerson, R. Alicki, and K. Życzkowski, Journal of Optics B: Quantum and Semiclassical Optics **7**, S347 (2005).

[11] A. W. Cross, L. S. Bishop, S. Sheldon, P. D. Nation, and J. M. Gambetta, Physical Review A **100**, 032328 (2019).

[12] J. M. Pino, J. M. Dreiling, C. Figgatt, J. P. Gaebler, S. A. Moses, M. S. Allman, C. H. Baldwin, M. Foss-Feig, D. Hayes, K. Mayer, C. Ryan-Anderson, and B. Neyenhuis, (2020), arXiv:2003.01293 .

[13] S. T. Flammia and Y.-K. Liu, Physical Review Letters **106**, 230501 (2011).

[14] A. Elben, R. Kueng, H.-Y. R. Huang, R. van Bijnen, C. Kokail, M. Dalmonte, P. Calabrese, B. Kraus, J. Preskill, P. Zoller, and B. Vermersch, Physical Review Letters **125**, 200501 (2020).

[15] J. Eisert, M. Cramer, and M. B. Plenio, Reviews of Modern Physics **82**, 277 (2010).

[16] A. Nahum, J. Ruhman, S. Vijay, and J. Haah, Physical Review X **7**, 031016 (2017).

[17] X.-G. Wen, International Journal of Modern Physics B **32**, 1830010 (2018).

[18] O. Gühne and G. Tóth, Physics Reports **474**, 1 (2009).

[19] U. Schollwöck, Annals of Physics **326**, 96 (2011).

[20] R. Schmied, J.-D. Bancal, B. Allard, M. Fadel, V. Scarani, P. Treutlein, and N. Sangouard, Science **352**, 441 (2016).

[21] J.-D. Bancal, N. Gisin, Y.-C. Liang, and S. Pironio, Physical Review Letters **106**, 250404 (2011).

[22] J.-D. Bancal, N. Sangouard, and P. Sekatski, Phys. Rev. Lett. **121**, 250506 (2018).

[23] N. Friis, O. Marty, C. Maier, C. Hempel, M. Holzäpfel, P. Jurcevic, M. B. Plenio, M. Huber, C. Roos, R. Blatt, and B. Lanyon, Physical Review X **8**, 021012 (2018).

[24] R. Horodecki, P. Horodecki, M. Horodecki, and K. Horodecki, Reviews of Modern Physics **81**, 865 (2009).

[25] R. Horodecki and M. Horodecki, Physical Review A **54**, 1838 (1996).

[26] S. Abe and A. Rajagopal, Physica A: Statistical Mechanics and its Applications **289**, 157 (2001).

[27] M. B. Hastings, I. González, A. B. Kallin, and R. G. Melko, Physical Review Letters **104**, 157201 (2010).

[28] P. Calabrese and J. Cardy, Journal of Statistical Mechanics: Theory and Experiment **2004**, P06002 (2004).

[29] S. Humeniuk and T. Roscilde, Physical Review B **86**, 235116 (2012).

[30] A. Kitaev and J. Preskill, Physical Review Letters **96**, 110404 (2006).

[31] M. Levin and X. G. Wen, Physical Review Letters **96**, 110405 (2006).

[32] S. T. Flammia, A. Hamma, T. L. Hughes, and X. G. Wen, Physical Review Letters **103**, 1 (2009).

[33] Y. Zhang, T. Grover, A. Turner, M. Oshikawa, and A. Vishwanath, Physical Review B **85**, 235151 (2012).

[34] X. G. Wen, International Journal of Modern Physics B **04**, 239 (1990).

[35] H.-c. Jiang, Z. Wang, and L. Balents, Nature Physics **8**, 902 (2012).

[36] P. Calabrese and J. Cardy, Journal of Statistical Mechanics: Theory and Experiment **2005**, P04010 (2005).

[37] D. M. Basko, I. L. Aleiner, and B. L. Altshuler, Annals of Physics **321**, 1126 (2006).

[38] J. H. Bardarson, F. Pollmann, and J. E. Moore, Physical Review Letters **109**, 017202 (2012).

[39] C. M. Alves and D. Jaksch, Physical Review Letters **93**, 110501 (2004).

[40] A. J. Daley, H. Pichler, J. Schachenmayer, and P. Zoller, Physical Review Letters **109**, 020505 (2012).

[41] R. Islam, R. Ma, P. M. Preiss, M. Eric Tai, A. Lukin, M. Rispoli, and M. Greiner, Nature **528**, 77 (2015).

[42] A. M. Kaufman, M. E. Tai, A. Lukin, M. Rispoli, R. Schittko, P. M. Preiss, and M. Greiner, Science **353**, 794 (2016).

[43] T. Brydges, A. Elben, P. Jurcevic, B. Vermersch, C. Maier, B. P. Lanyon, P. Zoller, R. Blatt, and C. F. Roos, Science **364**, 260 (2019).

[44] S. J. Van Enk and C. W. Beenakker, Physical Review Letters **108**, 110503 (2012).

[45] A. Elben, B. Vermersch, M. Dalmonte, J. I. Cirac, and P. Zoller, Physical Review Letters **120**, 050406 (2018).

[46] B. Vermersch, A. Elben, M. Dalmonte, J. I. Cirac, and P. Zoller, Physical Review A **97**, 023604 (2018).

[47] A. Elben, B. Vermersch, C. F. Roos, and P. Zoller, Physical Review A **99**, 052323 (2019).

[48] B. Vermersch, A. Elben, L. M. Sieberer, N. Y. Yao, and P. Zoller, Physical Review X **9**, 021061 (2019).

[49] M. K. Joshi, A. Elben, B. Vermersch, T. Brydges, C. Maier, P. Zoller, R. Blatt, and C. F. Roos, Physical Review Letters **124**, 240505 (2020).

[50] A. Elben, J. Yu, G. Zhu, M. Hafezi, F. Pollmann, P. Zoller, and B. Vermersch, Science Advances **6**, eaaz3666 (2020).

[51] Z.-P. Cian, H. Dehghani, A. Elben, B. Vermersch, G. Zhu, M. Barkeshli, P. Zoller, and M. Hafezi, Physical Review Letters **126**, 050501 (2021).

[52] S. Aaronson, in *Proceedings of the 50th Annual ACM SIGACT Symposium on Theory of Computing - STOC 2018*, STOC 2018 (ACM Press, New York, New York, USA, 2018) pp. 325–338.

[53] H.-Y. Huang, R. Kueng, and J. Preskill, Nature Physics **16**, 1050 (2020).

[54] F. Haake, *Springer Series in Synergetics*, Vol. 54 (Springer, 2010).

[55] F. Mezzadri, Notices Am. Math. Soc. **54**, 592 (2006).

[56] M. Ohliger, V. Nesme, and J. Eisert, New Journal of Physics **15**, 015024 (2013).

[57] C. Dankert, R. Cleve, J. Emerson, and E. Livine, Physical Review A **80**, 012304 (2009).

[58] B. Collins and P. Śniady, Communications in Mathematical Physics **264**, 773 (2006).

[59] R. Blatt and C. F. Roos, Nature Physics **8**, 277 (2012).

[60] Y. Nakata, C. Hirche, M. Koashi, and A. Winter, Physical Review X **7**, 021006 (2017).

[61] L. Banchi, D. Burgarth, and M. J. Kastoryano, Physical Review X **7**, 041015 (2017).

[62] W. Hoeffding, The Annals of Mathematical Statistics **19**, 293 (1948).

[63] A. Elben and B. Vermersch, Zenodo 10.5281/zenodo.3963878 (2020).

[64] B. Vermersch and J. C. Garreau, Physical Review E **85**, 046213 (2012).

[65] A. Elben, B. Vermersch, R. van Bijnen, C. Kokail, T. Brydges, C. Maier, M. K. Joshi, R. Blatt, C. F. Roos, and P. Zoller, Physical Review Letters **124**, 010504 (2020).

[66] S. H. Shenker and D. Stanford, Journal of High Energy Physics **2014**, 67 (2014).

[67] P. Hosur, X.-L. Qi, D. A. Roberts, and B. Yoshida, Journal of High Energy Physics **2016**, 4 (2016).

[68] S. Sachdev and J. Ye, Physical Review Letters **70**, 3339 (1993).

[69] A. Kitaev, A simple model of quantum holography. KITP strings seminar and Entanglement 2015 program.

[70] J. Maldacena, S. H. Shenker, and D. Stanford, Journal of High Energy Physics **2016**, 106 (2016).

[71] R. Fan, P. Zhang, H. Shen, and H. Zhai, Science Bulletin **62**, 707 (2017).

[72] X. Chen, T. Zhou, D. A. Huse, and E. Fradkin, Annalen der Physik **529**, 1600332 (2017).

[73] A. Bohrdt, C. B. Mendl, M. Endres, and M. Knap, New Journal of Physics **19**, 063001 (2017).

[74] Y. Huang, Y.-L. Zhang, and X. Chen, Annalen der Physik **529**, 1600318 (2017).

[75] A. Nahum, S. Vijay, and J. Haah, Physical Review X **8**, 021014 (2018).

[76] C. W. von Keyserlingk, T. Rakovszky, F. Pollmann, and S. L. Sondhi, Physical Review X **8**, 021013 (2018).

[77] M. Gärttner, J. G. Bohnet, A. Safavi-Naini, M. L. Wall, J. J. Bollinger, and A. M. Rey, Nature Physics **13**, 781 (2017).

[78] J. Li, R. Fan, H. Wang, B. Ye, B. Zeng, H. Zhai, X. Peng, and J. Du, Physical Review X **7**, 031011 (2017).

[79] B. Swingle, G. Bentsen, M. Schleier-Smith, and P. Hayden, Physical Review A **94**, 040302 (2016).

[80] G. Zhu, M. Hafezi, and T. Grover, Physical Review A **94**, 062329 (2016).

[81] N. Y. Yao, F. Grusdt, B. Swingle, M. D. Lukin, D. M. Stamper-Kurn, J. E. Moore, and E. A. Demler, arXiv:1607.01801 .

[82] X. Nie, Z. Zhang, X. Zhao, T. Xin, D. Lu, and J. Li, (2019), arXiv:1903.12237 .

[83] Y.-C. Liang, Y.-H. Yeh, P. E. M. F. Mendonça, R. Y. Teh, M. D. Reid, and P. D. Drummond, Reports on Progress in Physics **82**, 076001 (2019).

[84] R. Jozsa, Journal of Modern Optics **41**, 2315 (1994).

[85] M. P. da Silva, O. Landon-Cardinal, and D. Poulin, Physical Review Letters **107**, 210404 (2011).

[86] M. Heyl, EPL (Europhysics Letters) **125**, 26001 (2019).

[87] R. M. Lynden-Bell and H. M. Mcconnell, The Journal of Chemical Physics **37**, 794 (1962).

[88] W. P. Su, J. R. Schrieffer, and A. J. Heeger, Physical Review Letters **42**, 1698 (1979).

[89] K. Hida, Physical Review B **45**, 2207 (1992).

[90] S. De Léséleuc, V. Lienhard, P. Scholl, D. Barredo, S. Weber, N. Lang, H. P. Büchler, T. Lahaye, and A. Browaeys, Science **365**, 775 (2019).

[91] D. González-Cuadra, P. R. Grzybowski, A. Dauphin, and M. Lewenstein, Physical Review Letters **121**, 090402 (2018).

[92] D. González-Cuadra, A. Dauphin, P. R. Grzybowski, P. Wójcik, M. Lewenstein, and A. Bermudez, Physical Review B **99**, 045139 (2019).

[93] F. D. Haldane, Physical Review Letters **50**, 1153 (1983).

[94] V. L. Ginzburg and L. D. Landau, in *On Superconductivity and Superfluidity* (Springer Berlin Heidelberg, Berlin, Heidelberg, 2008) pp. 113–137.

[95] X. Chen, Z. C. Gu, Z. X. Liu, and X. G. Wen, Science **338**, 1604 (2012).

[96] X. Chen, Z.-C. Gu, Z.-X. Liu, and X.-G. Wen, Physical Review B **87**, 155114 (2013).

[97] J. Haegeman, D. Perez-Garcia, I. Cirac, and N. Schuch, Physical Review Letters **109**, 050402 (2012).

[98] F. Pollmann and A. M. Turner, Physical Review B **86**, 125441 (2012).

[99] K. Shiozaki and S. Ryu, Journal of High Energy Physics **2017**, 100 (2017).

[100] H. Shapourian, K. Shiozaki, and S. Ryu, Physical Review Letters **118**, 216402 (2017).

[101] N. Goldman, J. C. Budich, and P. Zoller, Nature Physics **12**, 639 (2016).

[102] F. Grusdt, N. Y. Yao, D. Abanin, M. Fleischhauer, and E. Demler, Nature Communications **7**, 11994 (2016).

[103] C. Repellin and N. Goldman, Physical Review Letters **122**, 166801 (2019).

[104] C. Repellin, J. Léonard, and N. Goldman 10.1103/PhysRevA.102.063316 (2020).

[105] J. Motruk and I. Na, Physical Review Letters **125**, 236401 (2020).

[106] H. Dehghani, Z.-P. Cian, M. Hafezi, and M. Barkeshli, (2020), arXiv:2005.13677 .

[107] Q. Niu, D. J. Thouless, and Y.-S. Wu, Physical Review B **31**, 3372 (1985).

[108] K. Shiozaki, H. Shapourian, K. Gomi, and S. Ryu, Physical Review B **98**, 035151 (2018).

[109] A. Peres, Physical Review Letters **77**, 1413 (1996).

[110] M. Horodecki, P. Horodecki, and R. Horodecki, Physics Letters A **223**, 1 (1996).

[111] G. Vidal and R. F. Werner, Physical Review A **65**, 032314 (2002).

[112] P. Calabrese, J. Cardy, and E. Tonni, Physical Review Letters **109**, 130502 (2012).

[113] P. Calabrese, J. Cardy, and E. Tonni, Journal of Statistical Mechanics: Theory and Experiment **2013**, P02008 (2013).

[114] A. Coser, E. Tonni, and P. Calabrese, Journal of Statistical Mechanics: Theory and Experiment **2014**, P12017 (2014).

[115] P. Ruggiero, V. Alba, and P. Calabrese, Physical Review B **94**, 035152 (2016).

[116] Y. Javanmard, D. Trapin, S. Bera, J. H. Bardarson, and M. Heyl, New Journal of Physics **20**, 083032 (2018).

[117] X. Turkeshi, P. Ruggiero, and P. Calabrese, Physical Review B **101**, 064207 (2020).

[118] H. Shapourian, P. Ruggiero, S. Ryu, and P. Calabrese, SciPost Physics **7**, 037 (2019).

[119] V. Alba and P. Calabrese, EPL (Europhysics Letters) **126**, 60001 (2019).

[120] V. Alba and P. Calabrese, Physical Review B **100**, 115150 (2019).

[121] V. Alba and F. Carollo, (2020), arXiv:2002.09527 .

[122] J. Kudler-Flam, M. Nozaki, S. Ryu, and M. T. Tan, Journal of High Energy Physics **2020**, 31 (2020).

[123] C.-M. Chung, V. Alba, L. Bonnes, P. Chen, and A. M. Läuchli, Physical Review B **90**, 064401 (2014).

[124] K.-H. Wu, T.-C. Lu, C.-M. Chung, Y.-J. Kao, and T. Grover, Physical Review Letters **125**, 140603 (2020).

[125] E. Wybo, M. Knap, and F. Pollmann, Physical Review B **102**, 064304 (2020).

[126] J. Gray, L. Banchi, A. Bayat, and S. Bose, Physical Review Letters **121**, 150503 (2018).

[127] Y. Zhou, P. Zeng, and Z. Liu, Physical Review Letters **125**, 200502 (2020).

[128] M. Planitz, W. H. Press, B. P. Flannery, S. A. Teukolsky, and W. T. Vetterling, *The Mathematical Gazette*, 3rd ed., Vol. 71 (Cambridge University Press, New York, NY, USA, 1987) p. 245.

[129] L. Pezzé and A. Smerzi, Physical Review Letters **102**, 100401 (2009).

[130] D. Girolami and B. Yadin, Entropy **19**, 124 (2017).

[131] N. Wyderka and O. Guehne, Journal of Physics A: Mathematical and Theoretical 10.1088/1751-8121/ab7f0a (2020).

[132] L. Knips, J. Dziewior, W. Kłobus, W. Laskowski, T. Paterek, P. J. Shadbolt, H. Weinfurter, and J. D. A. Meinecke, npj Quantum Information **6**, 51 (2020).

[133] C. Eltschka and J. Siewert, Physical Review A **101**, 022302 (2020).

[134] X. Mi, B. Vermersch, A. Elben, P. Roushan, Y. Chen, P. Zoller, and V. Smelyanskiy, Bulletin of the American Physical Society (2020).

[135] I. Frérot and T. Roscilde, Physical Review Letters **116**, 190401 (2016).

[136] P. Fromholz, G. Magnifico, V. Vitale, T. Mendes-Santos, and M. Dalmonte, Physical Review B **101**, 085136 (2020).

[137] J. Y. Choi, S. Hild, J. Zeiher, P. Schauß, A. Rubio-Abadal, T. Yefsah, V. Khemani, D. A. Huse, I. Bloch, and C. Gross, Science **352**, 1547 (2016).

[138] C. Carcy, H. Cayla, A. Tenart, A. Aspect, M. Mancini, and D. Clément, Physical Review X **9**, 041028 (2019).

[139] S. Léger, J. Puertas-Martínez, K. Bharadwaj, R. Dassonneville, J. Delaforce, F. Foroughi, V. Milchakov, L. Planat, O. Buisson, C. Naud, W. Hasch-Guichard, S. Florens, I. Snyman, and N. Roch, Nature Communications **10**, 5259 (2019).

[140] G. Carleo and M. Troyer, Science **355**, 602 (2017).

[141] E. P. L. Van Nieuwenburg, Y. H. Liu, and S. D. Huber, Nature Physics **13**, 435 (2017).

[142] J. Carrasquilla and R. G. Melko, Nature Physics **13**, 431 (2017).

[143] J. Carrasquilla, G. Torlai, R. G. Melko, and L. Aolita, Nature Machine Intelligence **1**, 155 (2019).

[144] B. S. Rem, N. Käming, M. Tarnowski, L. Asteria, N. Fläschner, C. Becker, K. Sengstock, and C. Weitenberg, Nature Physics **15**, 917 (2019).

Appendix A

Curriculum vitae

Benoît Vermersch

Curriculum Vitae

Université Grenoble Alpes
Laboratoire de Physique et Modélisation des Milieux Condensés
UMR 5493 CNRS.
25 avenue des Martyrs, BP166 F-38042 Grenoble Cedex, France
✉ *benoit.vermersch@lpmmc.cnrs.fr*
bvermersch.github.io

Born August 18th 1986, in Saint Cyr l'École, France.

Current appointments

Sept 2019- **Assistant Professor (Maître de conférences)**, *Laboratoire de Physique et Modélisation des Milieux Condensés (LPMMC)*, Université Grenoble Alpes-CNRS, France.

Sept 2020- **Researcher**, *Institute of quantum optics and quantum information (IQOQI) of the Austrian Academy of science*, Part-time employment (10%), Innsbruck, Austria.

Research interests

Measurement protocols for many-body quantum systems.

Quantum simulation with dipolar systems (Rydberg atoms, trapped ions, superconducting quantum circuits).

Theory of quantum networks (Waveguide quantum electrodynamics).

Numerical tensor-network methods for quantum many-body systems.

Career and Education

Jun 2017-Aug 2019 **Senior scientist, Quantum optics theory group of Prof. Peter Zoller, IQOQI**, *University of Innsbruck*, Austria.

Oct 2013-Jun 2017 **Postdoctoral researcher, Quantum optics theory group of Prof. Peter Zoller**.

2010-2013 **PhD thesis under supervision of Jean-Claude Garreau**, *Université Lille 1*, France.
Dynamics of ultracold interacting bosons in disordered lattices : Effects of interactions on the Anderson localization and transitions. Defense : 2013 Sept. 23rd

2009–2010 **Master of Science**, *Université Paris XI*, Orsay, France.
Laser-matter interactions. Ranked 1st.

2006-2009 **Graduate school**, *École Polytechnique*, Palaiseau, France.

2004-2006 **Classes préparatoires**, *Lycée Sainte Geneviève MPSI-PSI**, Versailles, France.

Teaching

2020/2021 **Lectures on quantum algorithms at the university Grenoble Alpes (M2-nanophysics)**.

2019/2020, 2020/2021 **Classical mechanics (L1) and statistical physics (L3) at the university Grenoble-Alpes**.

2019 **Course on quantum networks for a PhD summer school at the university of Innsbruck**.

2011-2013 **Teaching assistant**, *Institute of technology. 192 hours*, Lille, France.
Classical mechanics - practical work (TP)

2007–2009 **Oral exams**, *Classes Préparatoires PCSI Lycée Ste Geneviève*, Versailles, France.

Presentations

— **Invited talks** at various international conferences and workshops (9 invited talks since 2016, 2 invited talks scheduled). Details available on bvermersch.github.io

— **Invited seminars** (14 invited seminars since 2016).

Supervision activities

— **Piero Naldesi (Oct. 2020-)**, percentage (100%). Post-doctoral fellow at the Institute for Quantum Optics and Quantum Information, Innsbruck. The project is funded by a grant of the Austrian Science Fundation, for which Benoît Vermersch is project-investigator (see below). The goal of Piero Naldesi's project is to study the use controlled randomized operations to improve the resolution of quantum atomic microscopes.

— **Aniket Rath (Oct. 2020-)**, percentage (50%). PhD on randomized measurement protocols for probing multipartite entanglement, co-supervision ('co-encadrement') with Cyril Branciard (Néel). Funding via the LANEF program.

— **Aniket Rath (2020)**, percentage (80%). Optimization of randomized measurement protocols, Master 2 internship at university Grenoble Alpes. co-supervision with Anna Minguzzi.

— **Andreas Elben (2017-2020)**, percentage (50%). PhD on randomized measurement protocols at the university of Innsbruck (defense : May 2020, official PhD supervisor : Peter Zoller). My role was to supervise Andreas on a daily/weekly basis and to provide expertise on numerical simulations and quantum optics theory. We published 9 articles together (c.f., list below), and filed one patent application. I also assisted Andreas for the writing of his PhD manuscript and the preparation of his defense. Estimated supervision time : 6 hours per week.

— **Pierre-Olivier Guimond (2016-2020)**, percentage (30%). PhD on chiral quantum optics at the university of Innsbruck (defense : May 2020, official supervisor : Peter Zoller). I worked with Pierre-Olivier as supervising post-doc during the second part of his PhD (2017-2020). We published 4 articles together. Estimated supervision time : 3 hours per week .

— **Clemens Dlaska (2016)**, percentage (50%). Master's degree at the university of Innsbruck (defense : May 2016). I was fully in charge of the supervision of Clemens's project on quantum information transfers via topological edge states (one article published).

— **Other co-supervision activities :** Berit Vogell (PhD, 2017, university of Innsbruck), Azadeh Mazloom (PhD, 2016, university of Innsbruck), Florent Scol (Master, 2013, university of Lille), Clément Martinache (Master, 2012, university of Lille).

Grants

— Recipient of an **Agence National de la Recherche** (ANR) young researcher's grant on quantum technologies (2020-2024) 'Probing and verifying large-scale quantum technologies via randomized measurements'.

— Recipient of a independent researcher grant of the **Austrian Science Fundation** (FWF) (2020-2023) 'Protocols for the classification of topological quantum phases'.

— LANEF PhD grant obtained by our applicant Aniket Rath, collaboration with Cyril Branciard (Néel) (2020-2023).

— In charge of the representation of the UQUAM ERC Synergy grant and the ARL SciNet project project for the Innsbruck node (2017-2019).

Other activities

— **Workshop organiszation** Second topical UQUAM workshop on entanglement, Innsbruck, 2018, and UQUAM Paris-Innsbruck workshop, 2017.

— **Referee activities** Physical Review Letters, Physical Review X, Physical Review A, Physical Review B, Journal of Physics B (IOP), Annelen der Physik, Quantum.

— **Patents**
US Patent Application 62/875,323 : Verification of preparation of ground states.
European Application PCT/EP2019/083701 : Method for comparing quantum states.